

Electrophysiological Classes of Cat Primary Visual Cortical Neurons In Vivo as Revealed by Quantitative Analyses

LIONEL G. NOWAK,¹ RONY AZOUZ,² MARIA V. SANCHEZ-VIVES,³ CHARLES M. GRAY,²
AND DAVID A. McCORMICK⁴

¹Unité de recherche Cerveau et Cognition, Centre National de la Recherche Scientifique Unité Mixte de Recherche 5549, Université Paul Sabatier, Toulouse, France; ²Center for Computational Biology, Montana State University, Bozeman, Montana; ³Instituto de Neurociencias, Universidad Miguel Hernández-Consejo Superior de Investigaciones, San Juan de Alicante, Spain; and ⁴Department of Neurobiology, Yale University School of Medicine, New Haven, Connecticut

Submitted 3 September 2002; accepted in final form 8 September 2002

Nowak, Lionel G., Rony Azouz, Maria V. Sanchez-Vives, Charles M. Gray, and David A. McCormick. Electrophysiological classes of cat primary visual cortical neurons in vivo as revealed by quantitative analyses. *J Neurophysiol* 89: 1541–1566, 2003; 10.1152/jn.00580.2002. To facilitate the characterization of cortical neuronal function, the responses of cells in cat area 17 to intracellular injection of current pulses were quantitatively analyzed. A variety of response variables were used to separate the cells into subtypes using cluster analysis. Four main classes of neurons could be clearly distinguished: regular spiking (RS), fast spiking (FS), intrinsic bursting (IB), and chattering (CH). Each of these contained significant subclasses. RS neurons were characterized by trains of action potentials that exhibited spike frequency adaptation. Morphologically, these cells were spiny stellate cells in layer 4 and pyramidal cells in layers 2, 3, 5, and 6. FS neurons had short-duration action potentials (<0.5 ms at half height), little or no spike frequency adaptation, and a steep relationship between injected current intensity and spike discharge frequency. Morphologically, these cells were sparsely spiny or aspiny nonpyramidal cells. IB neurons typically generated a low frequency (<425 Hz) burst of spikes at the beginning of a depolarizing current pulse followed by a tonic train of action potentials for the remainder of the pulse. These cells were observed in all cortical layers, but were most abundant in layer 5. Finally, CH neurons generated repetitive, high-frequency (350–700 Hz) bursts of short-duration (<0.55 ms) action potentials. Morphologically, these cells were layer 2–4 (mainly layer 3) pyramidal or spiny stellate neurons. These results indicate that firing properties do not form a continuum and that cortical neurons are members of distinct electrophysiological classes and subclasses.

INTRODUCTION

The ability to identify neuronal types is of fundamental importance to developing a cellular and network level understanding of the operations of the cerebral cortex. Cortical neurons can be identified by any of a wide variety of characteristics including laminar location, dendritic and axonal morphology, neurotransmitter content and receptors, axon conduction velocity, receptive field characteristics, and intrinsic electrophysiological properties. Knowledge about intrinsic electrophysiological properties is of primary importance, not

only as a tool to identify neurons, but also because they strongly influence the input-output relationships and operation of cortical neurons and circuits.

Multiple schemes have been proposed to classify cortical neurons on the basis of their discharge pattern and intrinsic membrane properties. Early extracellular recording studies in vivo differentiated cortical cells into two broad categories: those that had thin (or “fast”) action potentials and exhibited high spontaneous activity were termed “fast spiking” cells, while neurons with broader action potentials and lower levels of spontaneous activity were termed “regular spiking” cells (Mountcastle et al. 1969; Simons 1978). These cells were hypothesized to correspond to nonpyramidal and pyramidal neurons, respectively (Mountcastle et al. 1969). However, other studies performed in the motor cortex reported large differences in action potential width between two subtypes of pyramidal neurons, the slow (broad spikes) and fast (thin spikes) pyramidal tract cells (Baranyi et al. 1993b; Calvin and Sypert 1976; Deschênes et al. 1979; Stafstrom et al. 1984; Takahashi 1965). Intracellular recording combined with labeling techniques revealed that RS cells were often pyramidal or spiny stellate cells, while FS neurons showed morphological features of subtypes of inhibitory neurons (Ahmed et al. 1998; Azouz et al. 1997; Chagnac-Amitai et al. 1990; Chen et al. 1996a; Foehring et al. 1991; Gupta et al. 2000; Hirsch 1995; Kaneko et al. 1995; Kawaguchi 1995; Krimer and Goldman-Rakic 2001; Larkman and Mason 1990; McCormick et al. 1985, 1993; Neagele and Katz 1990; Pockberger 1991; Thomson et al. 1996; Tseng and Prince 1993; Zhou and Hablitz 1996).

Intra- and extracellular recording studies in vivo also emphasized the presence of burst firing in a subset of cortical neurons (e.g., Bair et al. 1994; Baranyi et al. 1993a; Calvin and Sypert 1976; Cattaneo et al. 1981; Dégenétais et al. 2002; Istvan and Zarzecki 1994; Nuñez et al. 1993; Pockberger 1991). Bursting, however, does not appear to be a feature homogeneous enough to characterize one single cell type, because multiple types of bursting neurons have been de-

Address for reprint requests: D. A. McCormick, Dept. of Neurobiology, Yale Univ. School of Medicine, 333 Cedar St., New Haven, CT 06510 (E-mail: david.mccormick@yale.edu).

The costs of publication of this article were defrayed in part by the payment of page charges. The article must therefore be hereby marked “advertisement” in accordance with 18 U.S.C. Section 1734 solely to indicate this fact.

scribed in terms of action potential width or intraburst frequency in different species and cortical areas. In vitro, one type of neuron generates inactivating bursts of action potentials in response to depolarization through intrinsic membrane mechanisms (Connors et al. 1982; Franceschetti et al. 1995; Jones and Heinemann 1988; Mason and Larkman 1990; McCormick et al. 1985; Tseng and Prince 1993). These intrinsically bursting (IB) neurons were often (but not always) large layer 5 pyramidal cells (McCormick et al. 1985; Chagnac-Amitai et al. 1990; Larkman and Mason 1990; Pockberger 1991; Wang and McCormick 1993; Franceschetti et al. 1995). Additional in vivo and in vitro recordings revealed another class of burst-generating neurons, called "chattering" cells (Brumberg et al. 2000; Gray and McCormick 1996; Steriade et al. 1998, 2001). These cells generate bursts with high intraburst frequency of relatively short-duration action potentials in a rhythmic fashion in response to both depolarizing current pulses as well as sensory stimulation (Gray and McCormick 1996). In visual cortex, these cells were found to be layer II/III pyramidal cells (Gray and McCormick 1996).

More recent in vitro studies described multiple subtypes of GABAergic neurons. Although many of these, especially basket and chandelier cells, exhibited the fast-spiking pattern of action potentials, many did not. The electrophysiological properties of GABAergic interneurons vary widely, with different studies reporting the existence of between two and eight different subtypes (Cauli et al. 1997, 2000; Foering et al. 1991; Gibson et al. 1999; Gupta et al. 2000; Hestrin and Armstrong 1996; Hirsch 1995; Kawaguchi 1995; Kawaguchi and Kubota 1997; Krimer and Goldman-Rakic 2001; Llinas et al. 1991; Steriade et al. 1998; Thomson et al. 1996). These differences in electrophysiological features are correlated with differences in morphological features and peptide and calcium binding protein content.

The identification of different neuronal subtypes facilitates relating data across studies, since the correlation of physiologically defined subtypes with other properties helps in predicting the likely morphology, laminar location, input-output synaptic connections, and functional properties of the recorded cell. For example, identifying a neuron as an FS cell indicates with high probability that the cell is a parvalbumin-containing GABAergic neuron, which likely synapses on the cell bodies and/or axon hillocks of nearby pyramidal cells (e.g., Somogyi 1977; Somogyi et al. 1983). However, the identification of the physiological subtype of cortical neurons, as it is traditionally done, has four marked problems:

The first is that electrophysiological properties are dependent at least in part on the environment, condition, and age of the animal. In vitro studies are particularly prone to variation, since nearly all parameters are under the control of the experimenter, including the thickness of the tissue (and therefore oxygenation and the degree to which morphological processes are maintained), the temperature, ionic environment, age, and so on (for some consequences of age and ionic environment on membrane properties and spontaneous activity see Brumberg et al. 2000; Kasper et al. 1994b; McCormick and Prince 1987; Sanchez-Vives and McCormick 2000; for in vivo extracellular ionic concentration see Hansen 1985; Massimini and Amzica 2001). The second problem relates to the skill and bias of the investigator in correctly and consistently applying the physiological criteria. The third problem stems from whether or not

the subjectively defined category exists as a distinct entity, or whether it is part of a continuum of physiological properties that vary in a continuous way within a larger population. Finally, in subjective classification schemes, the choice of a value from a given variable distribution as a boundary separating two different cell types is often somewhat arbitrary.

We have attempted to solve some of these limitations by using a *quantitative* method (cluster analysis of intracellularly recorded data from the *adult* cat primary visual cortex in vivo) to identify subgroups of neurons without a priori assignment of possible cell classes. We found that cortical cells in vivo form four primary classes that correspond to RS, FS, IB, and CH cells, with each of these four classes consisting of statistically significant subclasses. Once the different cell classes and subclasses are defined, we examine and illustrate which variables are most useful in the segregation of cells into their respective classes. Finally, we examine the morphological features and receptive field properties of the cells with respect to the electrophysiological classes they belong to.

METHODS

Cat preparation

All experiments were performed on anesthetized and paralyzed male or female adult cats (2–3 kg). The protocol for surgery has been given in previous publications (Gray and McCormick 1996; Sanchez-Vives et al. 2000) and is briefly summarized here. Anesthesia was induced with ketamine (12–15 mg/kg, im) and xylazine (1 mg/kg, im). After cannulation of a forelimb vein for perfusion and insertion of an endotracheal tube for ventilation, the cat was placed in a stereotaxic frame. For the remainder of the surgical procedure, the animal was ventilated with either a 2:1 mixture of nitrous oxide and oxygen combined with halothane (1.5%), or with oxygen and isoflurane (2.5%). To minimize cortical motion arising from the heartbeat and respiration, cisternal drainage and a bilateral pneumothorax were performed and the animal was suspended by the rib cage to the stereotaxic frame. All intracellular recordings were performed in area 17. A craniotomy (3–4 mm wide) was made above the representation of the area centralis of area 17. A small opening was made in the dura before recording.

Following surgery, the animal was paralyzed with pancuronium bromide (Pavulon, 0.3 mg/kg for induction followed by a constant intravenous perfusion at 0.3 mg/kg/h in Ringer solution containing 5% dextrose). The nictitating membranes were retracted using ophthalmic phenylephrine, and the pupils were dilated and accommodation paralyzed with ophthalmic atropine. The eyes were focused onto a computer monitor at either 57 or 114 cm using corrective, gas-permeable contact lenses. The area centralis and optic discs were localized using the tapetal reflection technique. During recording, anesthesia was maintained with 0.4–1% halothane or with 0.5–2% isoflurane. The heart rate, expiratory CO₂ concentration, rectal temperature, and blood O₂ concentration were monitored throughout the experiment and maintained at 150–180 bpm, 3–4%, 37–38°C, and >95%, respectively. The depth of anesthesia was adjusted so that noxious stimuli produced no observable changes in the EEG or heart rate. After the recording session, the animal was killed by a lethal injection of sodium pentobarbital. This protocol was approved by the Yale University and University of California Institutional Animal Care and Use Committees and conforms to the guidelines recommended in "Preparation and Maintenance of Higher Mammals During Neuroscience Experiments", National Institutes of Health publication No. 91–3207.

Recording and electrophysiological signal acquisition

Conventional sharp micropipettes were pulled on a P-80 micropipette puller (Sutter Instruments, Novato, CA) from medium-walled glass capillaries (1BF100, Sarasota, FL), filled with 2 M K^+ -acetate and 2% biocytin (Molecular Probe, Eugene, OR), and beveled to a final resistance of 50–100 M Ω on a Sutter Instruments beveller. After a microelectrode was positioned just above the cortical surface, stability was achieved by application of agar (4% in artificial cerebrospinal fluid) to the cortical surface before penetrating the cortex. Intracellular signals were amplified with an Axoclamp-2B amplifier (Axon Instruments, Foster City, CA). The signals were digitized for storage on video tape. Signals were also digitized and acquired on-line and off-line with a 1401 interface and Spike2 software (CED, Cambridge, UK). For examining action potential features, the sampling rate was 50 kHz. In parallel, the intracellular signal was filtered to isolate action potentials (band-pass 200–20,000 Hz) and fed into a window discriminator. The timing (10 μ s resolution) of the spikes was then acquired on-line. The resulting time series were used for analyzing the discharge properties of the neurons.

When classifying neurons according to their electrophysiological features, it is important that these properties be stable and representative of a healthy cell. Our criteria for a healthy and stable recording included a resting membrane potential negative to -55 mV, stable electrophysiological properties without the use of “retaining” currents, the ability to generate repetitive action potentials in response to depolarizing current pulses, and an input resistance >20 M Ω (2 fast spiking cells displayed input resistance lower than 20 M Ω , owing to exceptionally strong anomalous rectification; they were nevertheless maintained in the sample as they displayed perfectly healthy discharge patterns and were capable of firing at a very high rate). Periods during which either the membrane potential or the electrophysiological properties were not stable (e.g., immediately on impalement or as the recording was lost) were discarded. Intracellular recordings from putative axons (positive going only action potentials and low apparent input resistance) and dendrites (large and prolonged spikes generated in response to depolarizing current pulses) were excluded from the present analysis. Bridge balance was continuously monitored and adjusted accordingly.

Quantification of responses to current pulses and cluster analysis

Once a stable intracellular recording was obtained, square current pulses (usually 0.3 s duration) were injected through the recording micropipette to characterize the electrophysiological features of the cells. Input resistance was measured from the response to hyperpolarizing current pulses (-0.2 to -0.5 nA), after averaging responses to about 10 pulses to reduce noise. The membrane time constant was evaluated from the averaged trace by fitting a single exponential to the membrane potential decay.

Depolarizing current pulses of different intensities (usually 0.1–0.9 nA, in steps of 0.1 nA) were used to evoke suprathreshold activation (Fig. 1). The first step of the analysis was to determine if a neuron was burst-generating or not. This is reflected in the interspike interval histograms (ISIH; bin width = 1 ms): burst-generating neurons were characterized by a bimodal distribution of interspike intervals, or by an ISIH with two different slopes beyond the modal value (Fig. 2, C–F), whereas a unimodal ISIH with a monotonic decay characterizes nonbursting neurons (Fig. 2, A and B). Histograms using the log values of the interspike intervals (logISIHs) helped in visualizing if an ISIH was bimodal or unimodal by concentrating long interspike intervals to a narrow range (Fig. 2, insets) and were used to decide if a neuron was burst-generating or not. Because the dividing line separating unimodal from bimodal logISIHs was difficult to identify, we supplemented our semi-quantitative approach using discriminant analysis. This analysis was based on seven variables extracted from

the log values of the interspike intervals (logISIs): 1) the mean logISI; 2) the geometric mean of the logISI; 3) the logISI median; 4) the coefficient of variation (SD/mean); 5) the skewness of the logISI distribution; 6) the kurtosis of the logISI distribution; and 7) the interquartile range (the distance between the 1st and 3rd quartile of the logISI distribution).

Following this segregation into two broad categories corresponding to bursting and nonbursting neurons, we performed additional analyses on each group to further characterize the data. For bursting neurons, the gap in the bimodal logISIH parted the spikes between those that belong to the same burst and those that belong to different bursts or those that correspond to isolated, single spikes. We used this property to identify the first spike of each burst, the spikes that occurred during a burst, and the spikes that occurred outside the bursts. This allowed us to calculate the *intra-burst frequency*, the *interburst frequency*, the *number of spikes per burst*, the *percentage of spikes that occurred in bursts*, and a *burst inactivation index* corresponding to the percentage of bursts that occurred in the first half of the pulse versus the total number of bursts. This index provides an estimate of a burst inactivation mechanism. A value of 50% corresponds to a neuron that fires bursts of action potentials throughout the current pulse, while a value of 100% corresponds to a neuron that fired bursts only in the first half of the current pulse, i.e., of a neuron for which the burst generation mechanism inactivates as a function of time (see Figs. 1, C and D, and 2, E and F).

For all the cells, the action potential features were measured after averaging several (>10) action potentials together (Fig. 1). For burst-generating neurons, only the first spike of each burst was used for averaging. We also calculated the time differential of the voltage (dV/dt). The spike threshold time was defined as the point in the dV/dt that was 3 SD above the mean noise level calculated for the dV/dt trace before the action potential. The amplitude (height) of action potentials was measured from threshold. The spike width was measured as the width at half height. The positive and negative peaks in the dV/dt yield the maximum rate of depolarization and repolarization, respectively. A dV/dt ratio was calculated as maximum rate of fall divided by maximum rate of rise.

For all the cells, whether bursting or not, we calculated the relationship between injected current intensity and the total number of spikes per pulse (normalized by the pulse duration). Cells that did not display a significant correlation between these two variables were excluded from further analysis. The slope (in Hz/nA) of the linear regression characterizes the current-frequency relationship of the neuron (Fig. 3).

For all the cells, we also applied a measure of adaptation by taking the ratio of the number of spikes in the first 50 ms versus the number of spikes in the first 100 ms of the current pulse, expressed as a percentage (“Ada50” index). The less a cell adapts, the closer to 50% this value.

The adaptation properties of nonbursting neurons were characterized with more precision by calculating the instantaneous firing rate as a function of the time elapsed since the beginning of the pulse (Fig. 5). Due to the presence of high instantaneous intraburst firing rates, this type of analysis was not applied to burst-generating neurons. For each current intensity, the change in firing rate was derived from a single exponential fit to the data. The plateau of the exponential curve corresponds to the adapted firing rate (F_{ad}). The strength of adaptation (*adaptation index*) was quantified as $100 \times (1 - F_{ad}/F_1)$, where F_1 corresponds to the firing rate of the first interspike interval. The time constant of adaptation corresponds to the time constant derived from the exponential fit. For some cells (especially FS neurons), adequate fitting was not obtained and therefore no adaptation time constant was extracted. For these cells, F_{ad} was calculated as the mean firing rate for the last 100 ms of the current pulse and used to calculate the adaptation index. Data have been taken into account only when F_1 was above 60 Hz. Below this limit, the firing pattern appeared to be affected by spontaneous activity, as reflected by an increased vari-

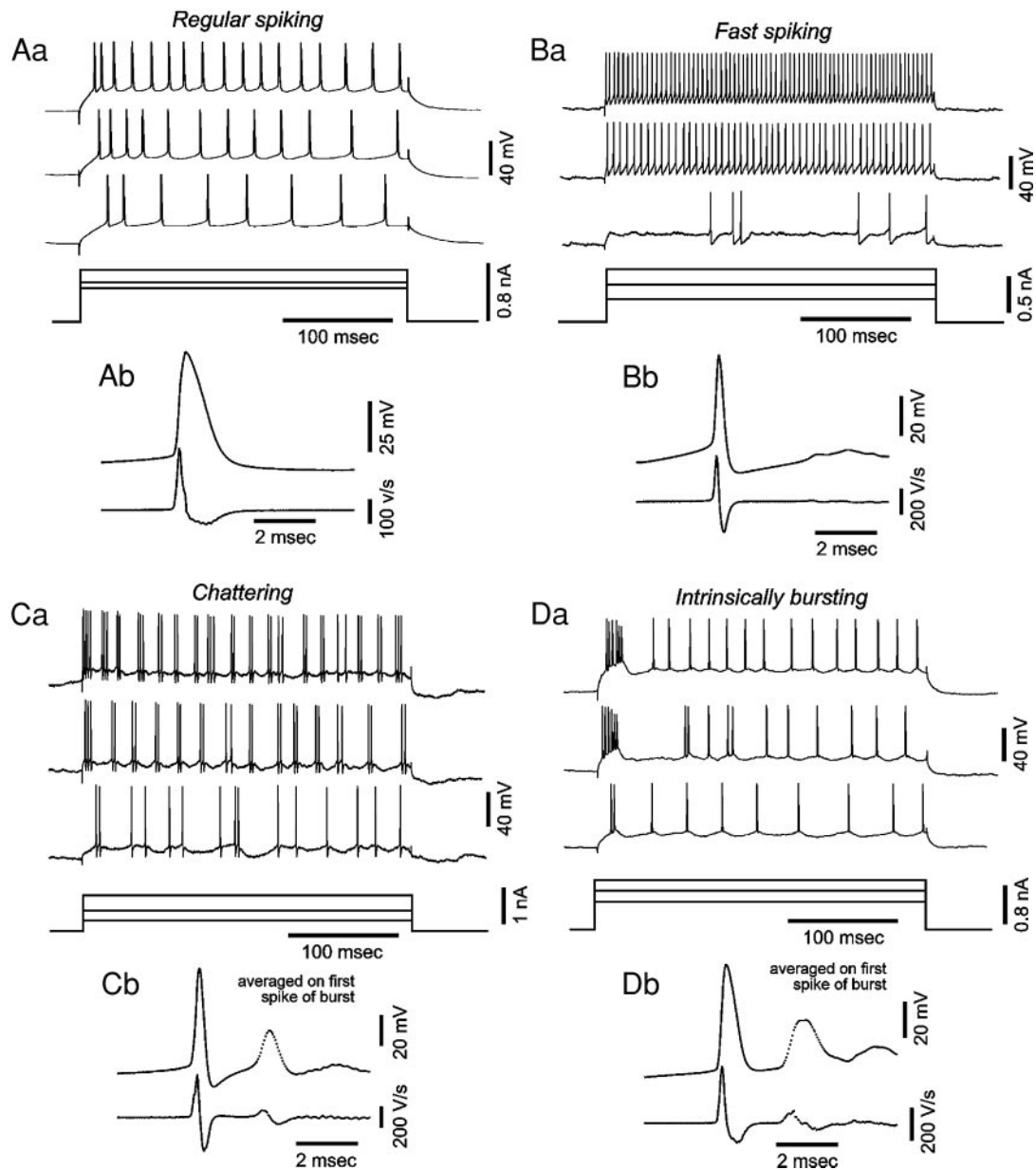


FIG. 1. Examples of action potential responses to depolarizing current injection in the 4 subjectively classified subtypes of cortical neuron. *A*: regular spiking (RS) cell. *B*: fast spiking (FS) cell. *C*: chattering (CH) cell. *D*: intrinsic bursting (IB) neuron. *Top* of each panel shows responses to 3 different current intensities. *Bottom plots* show average action potential and dV/dt . The individual action potentials and dV/dt in each panel are the result of averaging of ≥ 10 spikes. Therefore the amplitude and time course of the 2nd spikes in *Cb* and *Db* are not accurate, owing to jitter in the timing of these events.

ability in the distribution of adaptation-related values. For any given cell, values of adaptation strength and time constant obtained for each current intensity were thereafter averaged. (For specific cells, adaptation index and time constant varied with current intensity, but at the population level no consistent trend was observed.)

Cluster analysis was used to classify the cells by combining some of the variables described above. This method allowed us to classify the cells without a priori knowledge of the number of groups. Before performing the cluster analysis all variables were normalized to their z-scores. Some variables have not been used for the clustering and this requires some justification: the action potential height was not used as it could be influenced by the quality of the capacitance compensation, which itself depends on the depth of the electrode below the agar surface among other factors. The input resistance and time constant are reported here, but were not used in the cluster analysis, since in the

in vivo preparation ongoing activity is likely to affect these measures (e.g., Bernander et al. 1991; Destexhe and Pare 1999). Finally, when two variables were strongly correlated (for example, spike width and dV/dt ratio), only one was used for cluster analysis to avoid redundancy. Joining trees were constructed using Ward's method of amalgamation. The results of this classification method are plotted as a hierarchical tree (Fig. 6), in which the horizontal axis denotes the linkage distance calculated as Euclidean distance.

The result of the cluster analysis indicates the degree of similarity among neurons but does not assign statistical significance to the grouping. To determine whether the clusters contained cells with statistically distinct properties, we used the multiple ANOVA (MANOVA) test applied to the variables used to produce the clusters. For any pair of clusters, the Fisher's posthoc protected least significant difference (PLSD) test was thereafter applied to compare the means.

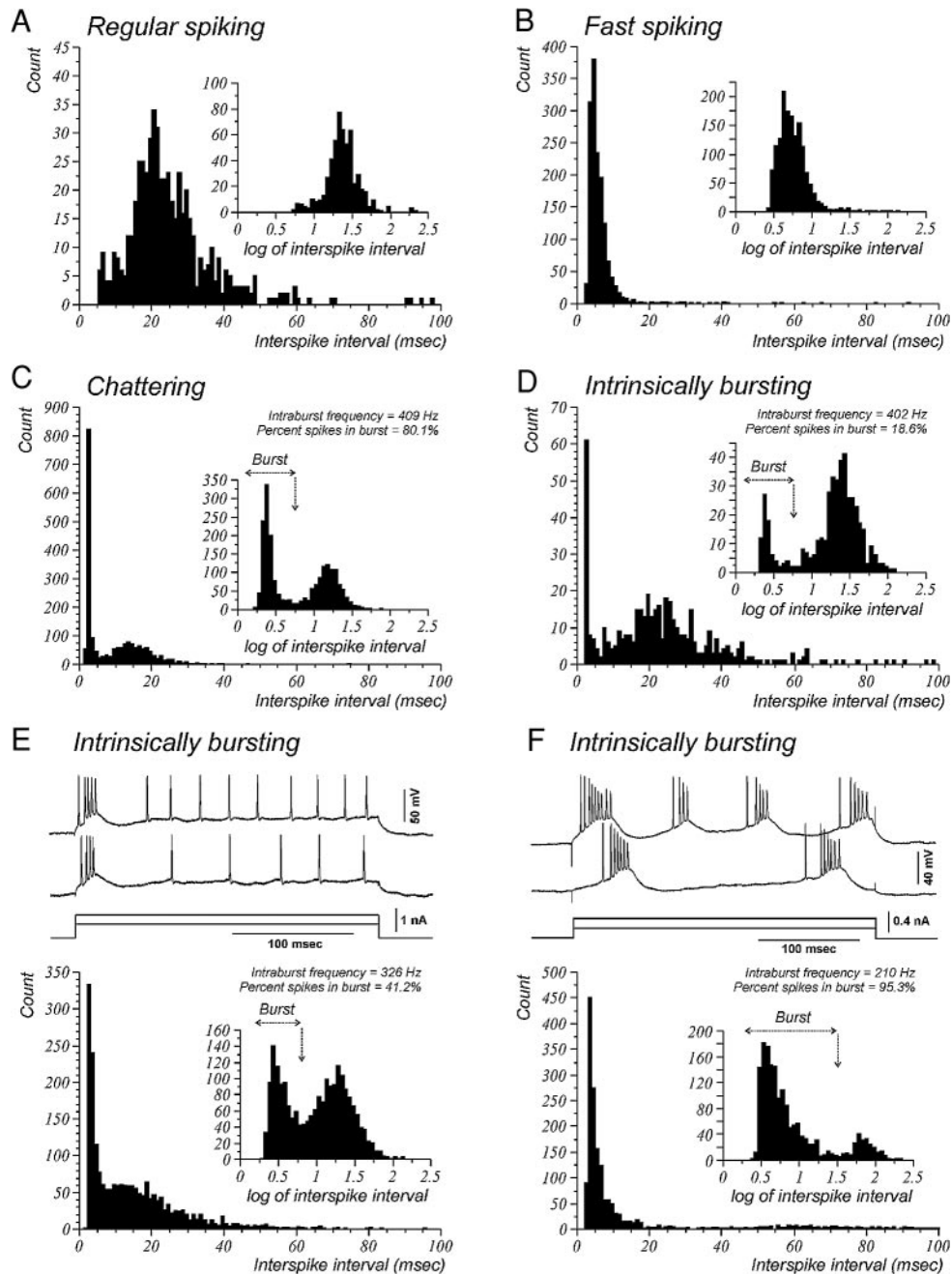


FIG. 2. Interspike interval histograms (ISI histograms) in bursting and nonbursting neurons. ISI histograms and histograms for the log values of the interspike intervals corresponding to the cells shown in Fig. 1 are presented in A–D. The logISI histogram better identifies bursting cells. E and F: additional examples of ISI histograms in 2 other bursting neurons, illustrating the diversity of cellular behavior. Examples of action potential response to current pulses are shown above each ISI histogram. Note in E and F that the bimodal nature of the ISI histogram is more clearly seen in the logISI histogram.

For variables not used to compute the cluster structure, either the posthoc PLSD Fisher's test or the classical *t*-test was used. All paired comparisons have also been made using the nonparametric, Mann-Whitney *U* test. In all cases, both parametric and nonparametric tests gave the same results (in terms of significance of differences) and the results obtained with the parametric tests are given. Unless mentioned, data are reported as mean \pm SD.

Receptive field properties

Three different methods have been used to determine if a receptive field was of the simple or complex category. First, the response to

small bars flashed within the receptive field was used to localize ON and OFF subregions (Hubel and Wiesel 1962). Cells exhibiting spatially nonoverlapping ON and OFF subfields, or a single ON or OFF subfield, were classified as simple, while cells showing clear overlap of the ON and OFF responses were classified as complex. Second, we used the peri-stimulus time histograms (PSTHs) obtained in response to broad drifting light and dark bars. Responses to the light-to-dark and dark-to-light edges did not overlap in simple cells, while they did overlap in the complex cells (Schiller et al. 1976). Third, we used the spike response to drifting sinusoidal gratings of various spatial frequencies to classify cells as simple or complex. For this purpose,

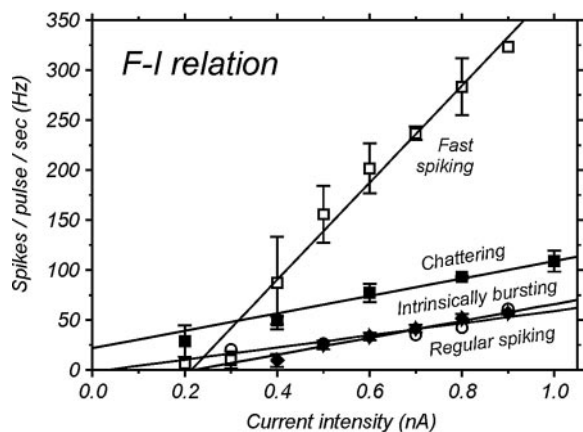


FIG. 3. Slope of firing rate vs. current intensity (f - I curves). Examples of f - I curves for the cells shown in Fig. 1. The slope of the relationship between injected current and mean firing rate during the current pulse is considerably steeper in the FS cell (519 Hz/nA) compared with that for the RS (85 Hz/nA), IB (56 Hz/nA), and CH (87 Hz/nA) cells. Each point is the average of the mean firing rate for 2–10 repeats of a given current intensity (only 1 repeat at 0.9 nA for the FS cell). Bars represent SE.

PSTHs were computed by taking the average response to one cycle of the grating. The amplitude of the DC component (F_0) and the first harmonic (F_1) at the temporal frequency of the stimulus were computed from the PSTH using Fourier analysis (after subtraction of the mean spontaneous activity level). For the spatial frequency that yielded the strongest response of either the F_0 or F_1 component, we calculated the ratio of F_1/F_0 to yield a “relative modulation index” (Skottun et al. 1991). The distribution of the relative modulation indices was bimodal, with a gap at 1. Based on this distribution, we considered cells as simple when the index was larger than 1 and complex when it was lower.

Histology

Following the experiment, the animal was given an overdose of sodium pentobarbital by intravenous injection and perfused with phosphate-buffered saline (PBS), followed by PBS containing 2–4% paraformaldehyde and 1.25% glutaraldehyde. After perfusion, the region of primary visual cortex containing the labeled cells was blocked and left in 30% sucrose until the tissue sunk. Coronal sections, 60–80 μ m thick, were cut on a freezing microtome. Biocytin staining was revealed using standard techniques (Horikawa and Armstrong 1988) with the Vectastain ABC kit from Vector (Burlingame, CA). Cortical layers were identified either through counter-staining or staining adjacent sections with cresyl violet, or by using Normarski optics and using standard measures and landmarks. Measurements have not been corrected for shrinkage.

RESULTS

During the performance of intracellular recordings in cat area 17 in vivo, a large number of neurons could be subjectively characterized as RS, FS, IB, or CH (e.g., Gray and McCormick 1996), while others appeared intermediate to these categories. Subjectively, RS neurons were identified based on their relatively broad action potentials (Fig. 1*Ab*) that exhibited spike frequency adaptation during injection of a constant depolarizing current pulse (Fig. 1*Aa*). FS cells exhibited thinner action potentials (Fig. 1*Bb*), apparently higher firing rates in response to depolarizing current pulses (Fig. 1*Ba*), and relatively little spike frequency adaptation (Fig. 1*Ba*).

CH cells were able to generate repetitive, high-frequency bursts of two or more relatively short-duration action potentials (Fig. 1*C, a* and *b*). Within each burst, each spike was followed by a fast afterhyperpolarization and an afterdepolarization (ADP; Fig. 1*C*). This ADP activated the next action potential in the burst. The bursts were terminated by the failure of the ADP to generate an action potential and were followed by a 15- to 100-ms afterhyperpolarization.

The final category of readily distinguishable neurons were the IB cells. These cells were distinguished from CH cells by their tendency to fire bursts of spikes only at the beginning of depolarizing current pulses (Fig. 1*Da*), and they rarely displayed repetitive bursting. Their action potentials were broader than those of CH cells (Fig. 1*Db*), and the frequency of firing during a burst appeared to be lower. Finally, the action potential amplitudes of IB neurons often decreased during the generation of a burst.

Figure 1 illustrates so called “typical” examples of each cell class for one possible classification scheme. However, in the overall population there was a large amount of variability in discharge pattern across cells, and some neurons exhibited properties intermediate to those illustrated. One intermediate behavior was the generation of repetitive burst discharges throughout the duration of the current pulse, like a CH neuron, but with bursts that were typical for that of an IB cell (Fig. 2*F*). Another intermediate behavior corresponded to cells that generated short-duration action potentials, like an FS cell, but displayed spike frequency adaptation like an RS cell. We also observed neurons that appeared similar to CH cells, but that only occasionally generated bursts of action potentials. Finally, RS cells differed in their adaptation properties, in that some cells adapted rapidly and/or strongly while other cells adapted slowly and/or weakly.

Do cells displaying these (and other) patterns of activity represent their own unique categories, or are they just members of those subjectively defined, but on one end of a continuum? In a related question, how many subgroups of neurons are there in our recordings from cat visual cortex?

To answer these questions, a more detailed quantitative analysis of the spike discharge patterns had to be conducted. To achieve this goal, we performed cluster analysis of the discharge parameters from a total of 220 cells recorded intracellularly in vivo in area 17. Among these cells, 48 were successfully labeled with biocytin and their morphology examined.

Quantitative analysis of electrophysiological properties

PARTITIONING BETWEEN BURSTING AND NONBURSTING NEURONS. The first step in our analysis was to decide whether a neuron was burst-generating or not. One essential aspect of bursting behavior is that an action potential occurring within a burst is not independent from the one that preceded it: in general (Fig. 1, *C* and *D*), the second action potential of a burst is triggered by an ADP resulting from the first action potential, and so on for each subsequent spike of the burst. One way to illustrate this type of dependence on a short (milliseconds) time scale is through the use of interspike interval histograms (ISIHS). These histograms show how often a spike is followed by another spike at a given interval.

The ISIHS (all current intensities have been pooled together)

for the cells shown in Fig. 1 are presented in Fig. 2, A–D. The ISIH for the RS cell (Fig. 2A) shows a refractory period of 5 ms. The ISIH is unimodal and skewed such that a larger number of ISIs are present on the right of the mode. The ISIH for the FS cell (Fig. 2B) shows a shorter refractory period and a mode displaced toward lower values in comparison to the RS cell. However, the ISIH in the FS cell also exhibits a monotonic decay beyond the peak.

Contrary to those described above, the ISIH of the CH cell is bimodal (Fig. 2C). One mode is centered on an interval value of 2.5 ms, indicating an increased probability of spiking within a few msec following each action potential. This corresponds to the ISIs within the bursts. The second mode is centered on a value of 14 ms, corresponding to the interval between the last spike of one burst and the first spike of the subsequent burst. The two peaks in the ISIH are separated by a clear gap at 6 ms. Finally, the ISIH of an IB neuron (Fig. 2D) also shows a bimodal distribution with a gap at 6 ms and two modes at 3 and 20 ms. These examples illustrate a fairly clear separation between bursting and nonbursting firing patterns.

In contrast to these examples, there were many neurons whose individual responses to current pulses were strongly suggestive of bursting behavior but whose ISIH could not be easily divided into unimodal or bimodal categories. For some cells, the gap was difficult to detect (Fig. 2E) or the ISIH did not display an obvious gap (Fig. 2F). In these cases, however, the distribution of the log of the ISIs (Fig. 2, insets) was clearly bimodal. Using the criteria of unimodal or bimodal distribution of logISIs, we classified all neurons into either bursting, or nonbursting cells. We checked the appropriateness of this

semi-quantitative approach by using discriminant analysis. Discriminant analysis was based on seven statistical parameters extracted from the log values of the interspike intervals (see METHODS). For only 18 of 220 cells did the discriminant analysis suggest a bursting/nonbursting classification differing from the one we inferred on the basis of logISIH shape. This number was reduced to 13 cells when the discriminant analysis was performed with the mean, the geometric mean, the skewness, and the median of the logISIs. Eleven of these 13 cells were initially classified as bursting. Thorough examination of ISIH, logISIH and individual responses to current pulses nevertheless indicated a clear bursting behavior in 8 of these 11 cells. Two of the 13 cells were initially classified as nonbursting and thorough examination of their response to current pulses convinced us to stick with our initial decision for one of these two cells. Thus altogether, only 4 of 220 cells remained ambiguous in their bursting behavior, or lack thereof. The discriminant analysis and logISIH criteria yielded a surprisingly good match, especially considering that none of the statistics extracted from the logISI directly measures the uni- or bimodality of the logISI distribution. We feel that the classification of cells into bursting and nonbursting groups based on logISIH plots provides an intuitive and sufficiently accurate segregation method to warrant its utilization.

VARIABLES USEFUL IN THE CLASSIFICATION OF NEURONS. The ISIHs and the statistics that can be extracted from the logISIs, although quite useful to distinguish bursting from nonbursting neurons, do not reflect all the intrinsic properties of cortical neurons. To obtain a more precise classification of cortical

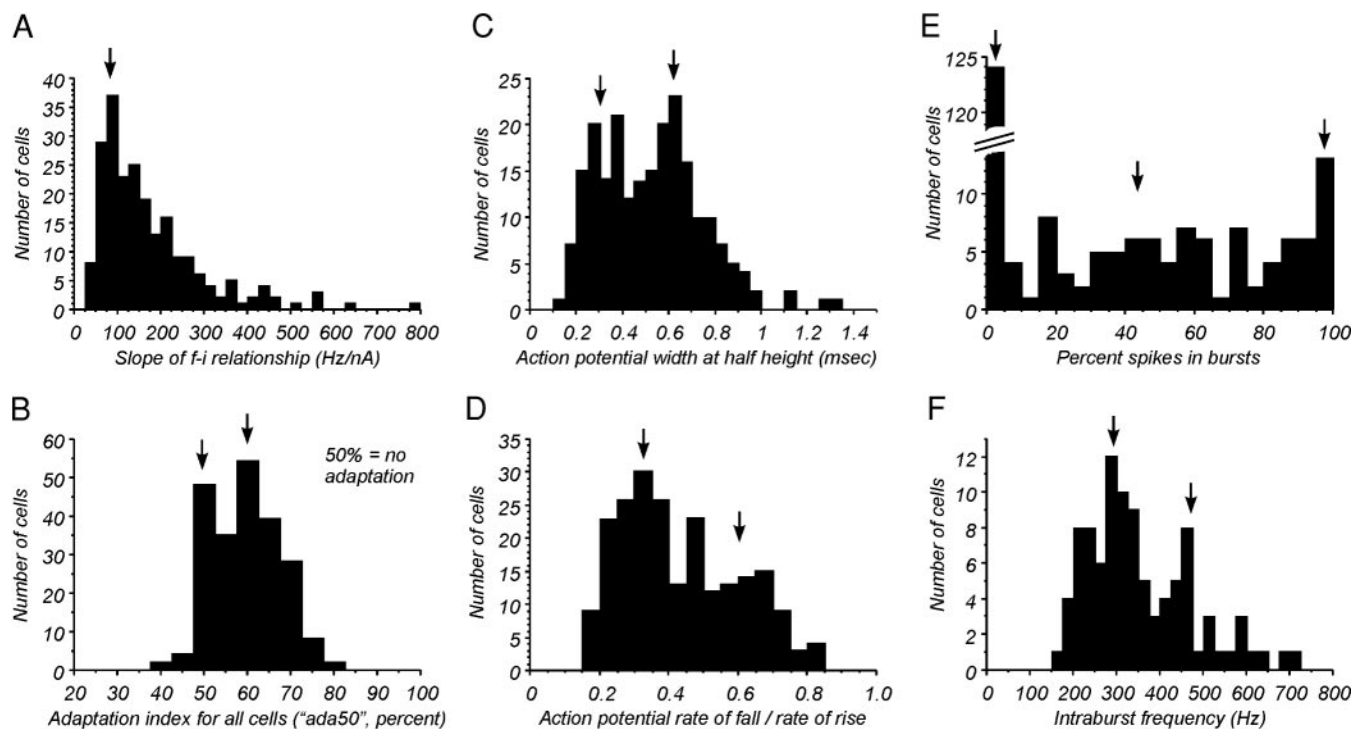


FIG. 4. Distributions obtained for some of the variables used for quantitative and subjective classification of cells. A: slope of the *f-I* relationship. B: distribution of adaptation indices (ada50). A value of 50% indicates the same number of spikes is present in the 1st and 2nd 50-ms epochs of the response (i.e., no adaptation). Values larger than 50% indicate adaptation in firing rate. C: distribution of action potential widths (measured at half height). D: ratio of the maximum rate of fall to the maximum rate of rise of the action potential. E: percentage of spikes in bursts. F: intraburst frequency (for burst-generating neurons only). Arrows point to possible modes in the distributions.

neurons, we analyzed other discharge properties that varied between different neurons.

One of these variables is the slope of the relationship between injected current intensity and firing rate (f - I relationship). The f - I relationship for the four cells of Fig. 1 are shown in Fig. 3. Of interest is the much steeper slope for the FS neuron compared with the other cells. To determine if the slope of the f - I relationship is useful in distinguishing between different subtypes of neurons, we plotted this value for the entire population (Fig. 4A). Although this distribution is not bimodal, it is skewed to the right. While 88% of the cells showed slope values lower than 300 Hz/nA, a minority of cells (12%) displayed slope values between 300 and >600 Hz/nA.

The distribution of values for several of the other variables capable of partitioning neurons into different populations are plotted in Fig. 4, B-F. The degree of spike frequency adapta-

tion ("ada50", Fig. 4B) corresponds to the ratio of the number of spikes in the first 50 ms of the response to a current pulse to the number of spikes in the first 100 ms of the current pulse. This ratio has been calculated for all the cells, both bursting and nonbursting. The distribution is suggestive of two possible peaks at 50% and 60% (Fig. 4B), indicating that there may be two populations with considerable overlap for this parameter.

The distribution of spike width measured at half height (Fig. 4C) may also possess two modes (0.3 and 0.6 ms), suggesting the existence of two groups of cells, one with thin (<0.4 ms) and another with broad (>0.4 ms) action potentials. The distribution of the ratio of the maximal rate of fall to the maximal rate of rise of the action potential also revealed a non-Gaussian distribution, with possible modes at around 0.3 and 0.65 (Fig. 4D).

The distribution of the percentage of spikes occurring during

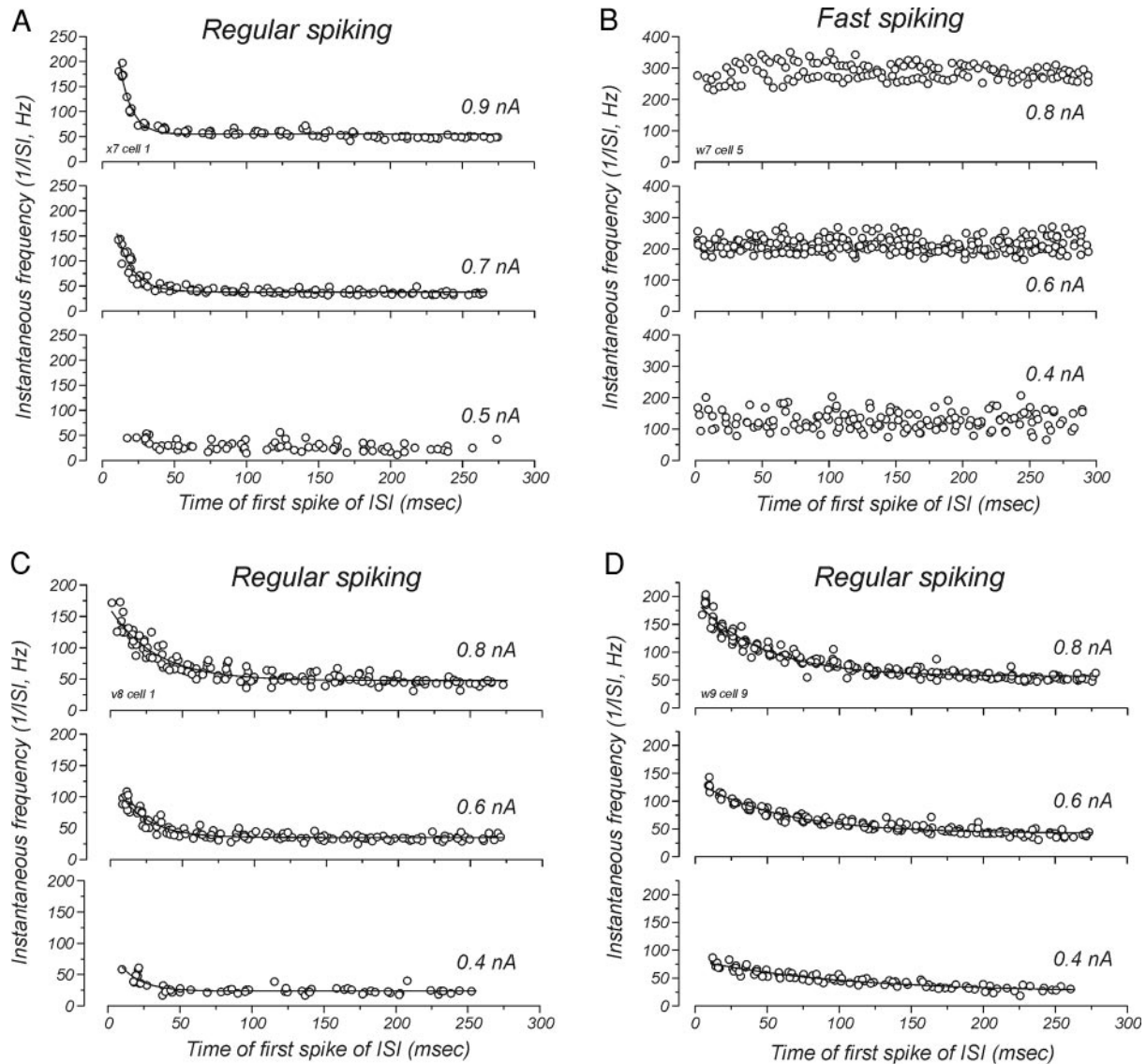


FIG. 5. Adaptation of action potential discharge in nonbursting neurons. *A*: instantaneous firing rate plotted as a function of time for the RS cell of Fig. 1*A*. Mean adaptation time constant is 14.9 ms. *B*: similar plot for the FS neuron of Fig. 1*B*. Note the lack of adaptation and overall higher discharge rate than in the cells of parts *A*, *C*, and *D*. *C* and *D*: adaptation in 2 additional RS cells, with intermediate (*C*, mean = 26.3 ms) and long (*D*, mean = 64.5 ms) adaptation time constants. For any given interspike interval and current intensity, several points appear superimposed due to the fact that several pulses with the same current intensity were used.

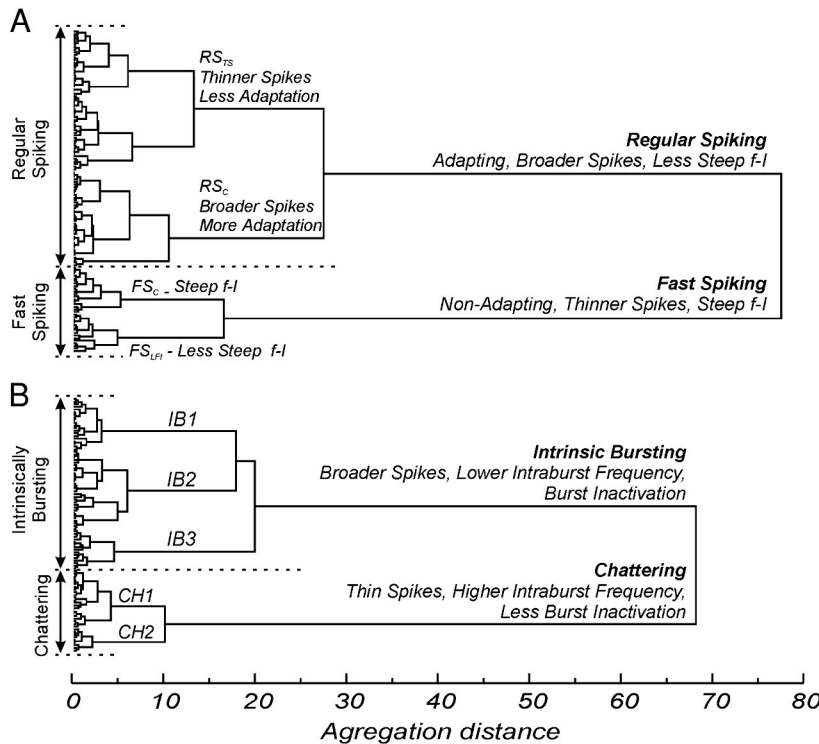


FIG. 6. Hierarchical tree plots illustrating the results of cluster analysis. *A*: dendrogram for nonbursting neurons. There are 2 main branches corresponding to RS and FS categories. Within the RS class, there are 2 subclasses, which we have termed RS_{TS} and RS_C . RS_{TS} cells exhibited thinner spikes and less spike frequency adaptation than RS_C cells. The main difference between the 2 subtypes of FS cells was the slope of their $f-I$ plot, with FS_{LF} cells having a less steep $f-I$ relation than FS_C cells. *B*: dendrogram for bursting neurons. The 2 main branches correspond to IB and CH cells. Three statistically significant subclasses of IB cells and 2 subclasses of CH cells are also considered.

bursts (Fig. 4E) suggests that cortical neurons may exhibit three distinct bursting behaviors, corresponding to cells that exhibit no bursts (<5%), cells whose spikes occur only during bursts (95–100%), and cells exhibiting intermediate values (5–95%).

Finally, for bursting neurons, the distribution of intraburst firing rates revealed a possible bimodal segregation with peaks at approximately 300 and 450 Hz (Fig. 4F).

While the distributions illustrated in Fig. 4 may suggest different groups of cells, by themselves they do not reveal

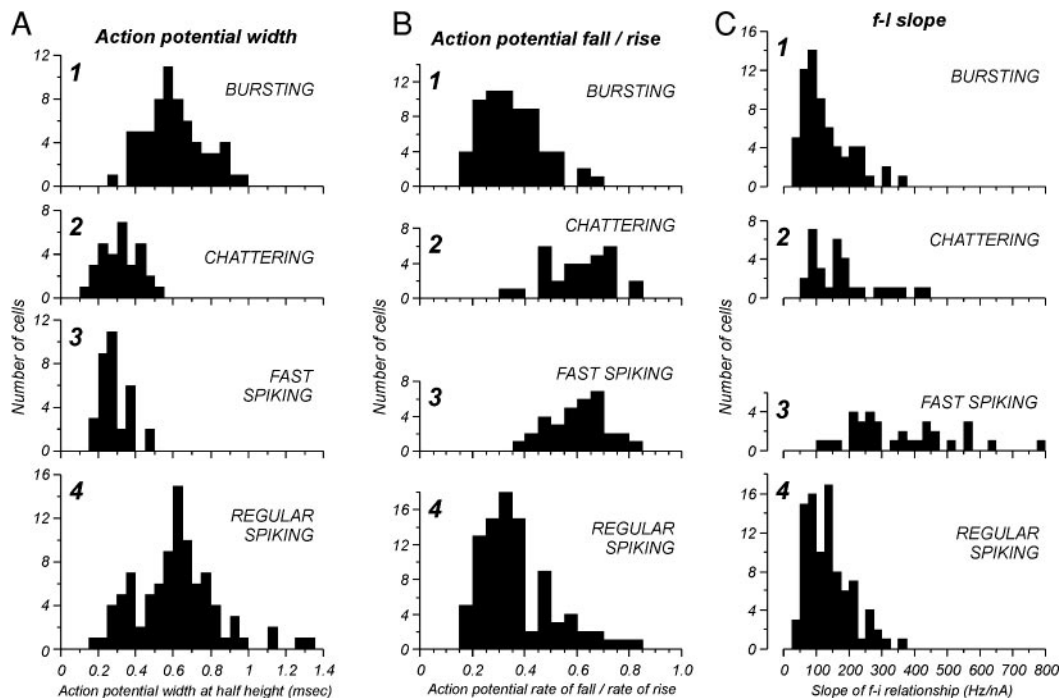


FIG. 7. Distribution of values for 3 variables measured in both bursting and nonbursting neurons. *A*: histograms of action potential width measured at half height for IB neurons (A1), CH cells (A2), FS cells (A3), and RS cells (A4). *B*: ratio of maximum rate of fall to maximum rate of rise of the action potential presented separately for the same 4 cell classes. Both FS and CH cells have thinner spikes than those of RS and IB neurons due to a faster rate of repolarization. *C*: histograms of the $f-I$ slopes for the RS, FS, IB, and CH cell classes. FS cells display the highest slope values, indicating a much higher gain between injected current and firing rate compared with the other 3 cell classes.

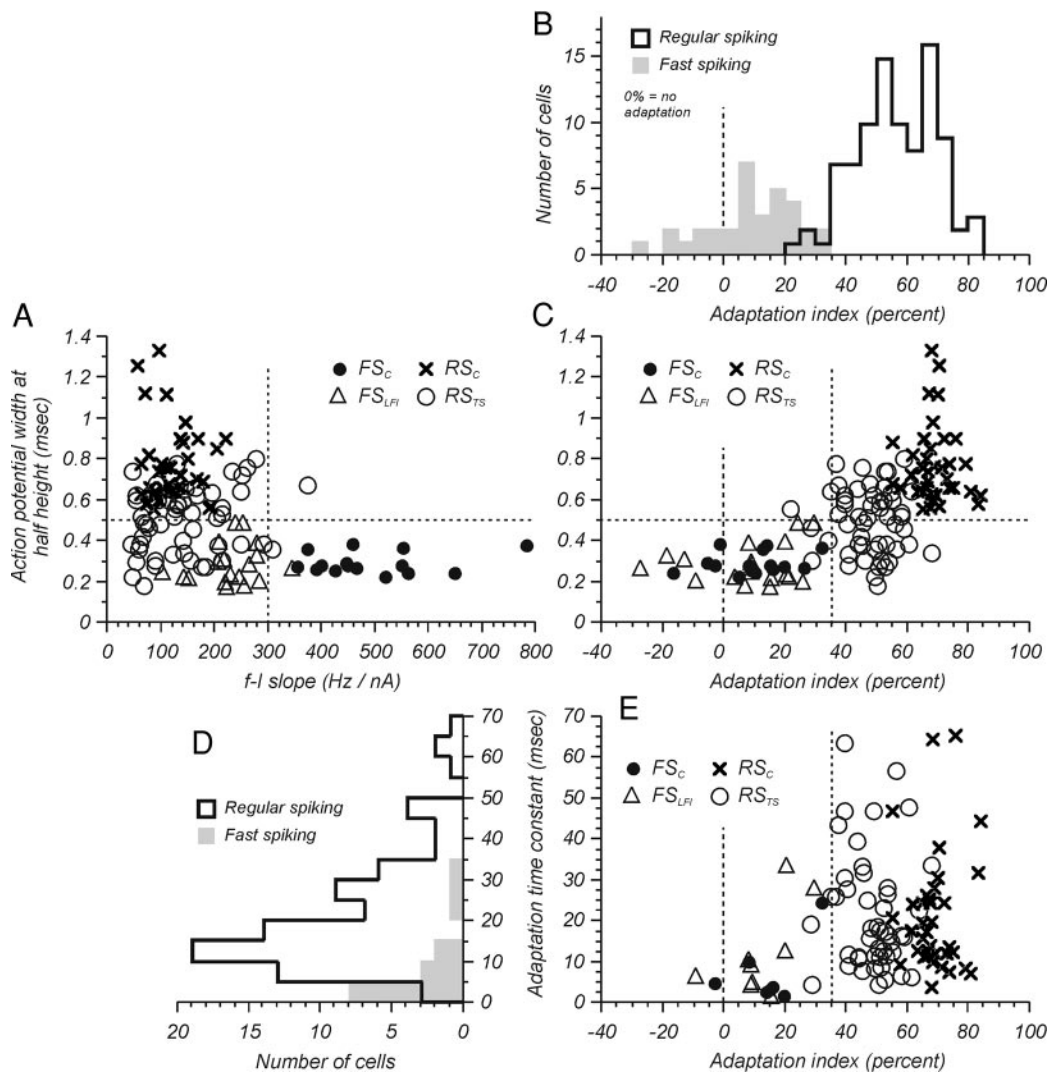


FIG. 8. Comparison of the properties of spike generation between fast spiking and regular spiking neurons. *A*: f -I slope plotted against action potential width for RS and FS cells. The distribution shows overlap of FS and RS cells when their action potential widths are <0.5 ms and their f -I slope values are <300 Hz/nA, indicating that these 2 variables alone do not cleanly separate FS and RS cells. The vertical dotted line delimits the f -I slope value (300 Hz/nA) beyond which only FS cells are encountered, and the horizontal dotted line delimits the action potential width (0.5 ms) beyond which only RS neurons are found. Subclasses of FS and RS are distinguished by different symbols to illustrate the thinner spikes in RS_{TS} cells and the highest f -I slope values in FS_C cells. *B*: histogram of adaptation indices illustrating a clear difference in firing rate adaptation between FS and RS neurons. Zero percent corresponds to no adaptation. Note overlap limited to adaptation index values between 20% and 35%. *C*: action potential widths plotted against adaptation indices. The quadrant defined by action potential width <0.5 ms and adaptation index $<35\%$ (dashed lines) contains all the FS cells and only 3 RS cells. *D*: histogram of adaptation time constants in RS and FS cells. *E*: adaptation time constants plotted against adaptation ratios shows that adaptation, when present, is faster and weaker in FS cells compared with RS cells. Two FS cells exhibited average negative adaptation ratios but showed spike frequency adaptation on some trials, and the time constant of adaptation was calculated from these trials. Adaptation time constant does not allow a separation between subclasses of RS and FS cells.

nonoverlapping populations of neurons. None of the individual variables that we measured reliably distinguished the subjectively defined cell groups. To determine if a *multi*-variable analysis could distinguish different cell classes, we performed cluster analysis of our data after separating the cells into bursting and nonbursting categories according to the logISIHS (Fig. 2). This allowed the use of variables that could be determined in one group but not the other.

CLUSTER ANALYSIS OF NONBURSTING NEURONS. For nonbursting neurons, we included the magnitude and time constant of firing rate adaptation as additional variables (Fig. 5). This adaptation was quantified by fitting the data relating instanta-

neous firing rate as a function of time with a single exponential function. The strength of adaptation (*adaptation index*) was calculated as $100 - (100 \times F_{ad}/F_1)$, where F_{ad} is the adapted firing rate (horizontal asymptote of exponential fit) and F_1 the firing rate for the first interspike interval. The adaptation index expresses the reduction in firing rate over time, with respect to the firing rate at the beginning of the current pulse. The adaptation time constant is derived from the time constant of the exponential fit. Values of the adaptation index and time constant were averaged across the different current intensities (for details see METHODS).

Three variables were selected in an effort to distinguish

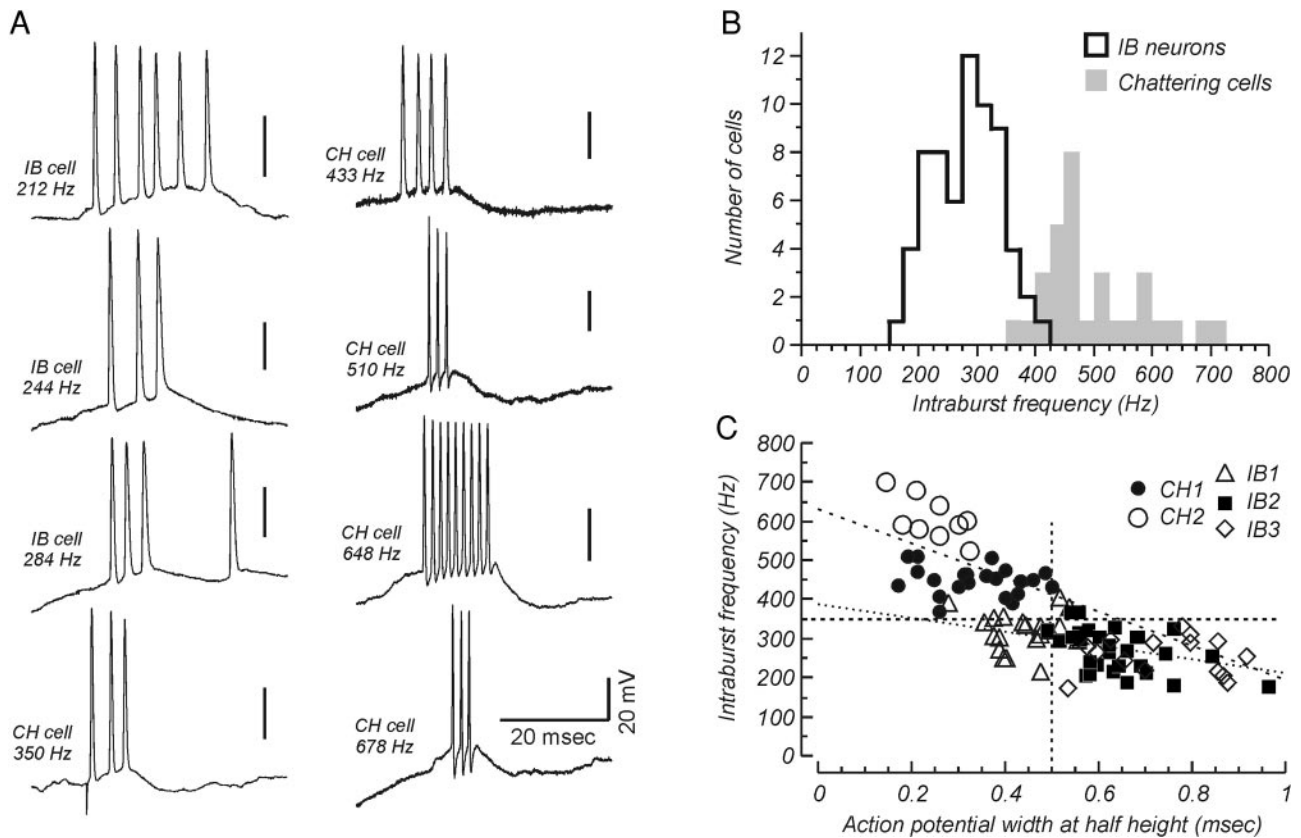


FIG. 9. Characteristics of action potential bursts in IB and CH cells. *A*: examples of single bursts from 8 different bursting neurons (3 IB and 5 CH cells) are shown. Note decreased spike width and more prominent fast AHP with increased intraburst frequency. *B*: histogram of intraburst firing rates. CH cells can be defined by intraburst frequency >425 Hz and IB neurons by intraburst frequency <350 Hz. Overlap between 350 and 425 Hz is limited to a small number of cells. *C*: correlation between intraburst frequency and action potential width at half height. The 2 parameters are significantly correlated, indicating that neurons with thinner action potentials generate bursts with higher intraburst firing rates. The slope of the correlation was steeper for CH cells (slope = -439 Hz/ms, $r^2 = 0.257$, $P = 0.003$) compared with IB neurons (slope = -176 Hz/ms, $r^2 = 0.231$, $P < 0.0001$). Note the scatter of data points for the CH cells where intraburst frequencies around 500 Hz are associated with action potential widths between 0.2 and 0.4 ms. CH neurons can be characterized as cells with intraburst frequencies >350 Hz and spike widths <0.5 ms. Subclasses of CH and IB neurons are identified by different symbols to illustrate differences in spike width and intraburst frequency.

different subtypes of nonbursting cells. These variables were action potential width (Fig. 1), the slope of the f - I relationship (Fig. 3), and the adaptation index (Fig. 5). Cluster analysis based on these three variables revealed two distinct subgroups that correspond closely to the RS and FS subjective classifications (84% agreement for both categories). The dendrogram of Fig. 6A shows that the branches corresponding to these two clusters separate at a large aggregation distance on the right.

Additional cluster analyses, which included the slope of the f - I relationship for the first interspike interval (f_1 - I), in combination with the three variables mentioned above, did not reveal additional well-separated clusters of neurons (data not shown). Instead, the RS and FS clusters were well maintained (3 cells changed cluster membership), but the aggregation distance between the origin of the tree and the first branch point was decreased to 69 instead of 78 as in Fig. 6A.

In Fig. 6A, the branch corresponding to RS cells divides at a distance of 26, leading to two subclasses of RS cells. These two subgroups contained neurons with properties that differed significantly (MANOVA test, $P < 0.0001$). The larger subclass contains cells with thinner spikes and less spike frequency adaptation (Fisher's PLSD test, $P < 0.0001$ for both param-

eters) and are termed here "thin spiking regular spiking" (RS_{TS}) neurons. The other RS subclass contains cells that display the "classical" characteristics of RS neurons, namely broader spikes and stronger spike frequency adaptation (termed here RS_C).

Within each of these two subclasses, additional subgroups were revealed that were also significantly different. In fact, MANOVA tests suggested significant differences even for clusters with very small separation distances. Thus for RS cells, it was possible to isolate 13 different clusters, having branch points at aggregation distances ≥ 2 , which contained cells whose properties differed significantly across clusters ($P < 0.0001$). These additional subgroups were not named, nor will they be considered further here, since the functional relevance of these subgroups is not yet known.

To determine the robustness of the two principal RS subclasses, we examined the effect of including the f_1 - I relation on their membership. The addition of this variable resulted in large changes in the membership of the subclasses, while the two main clusters (RS and FS) remained intact. Therefore, while the two main clusters appear to be quite robust, the subclusters are dependent on the variables used for cluster analysis.

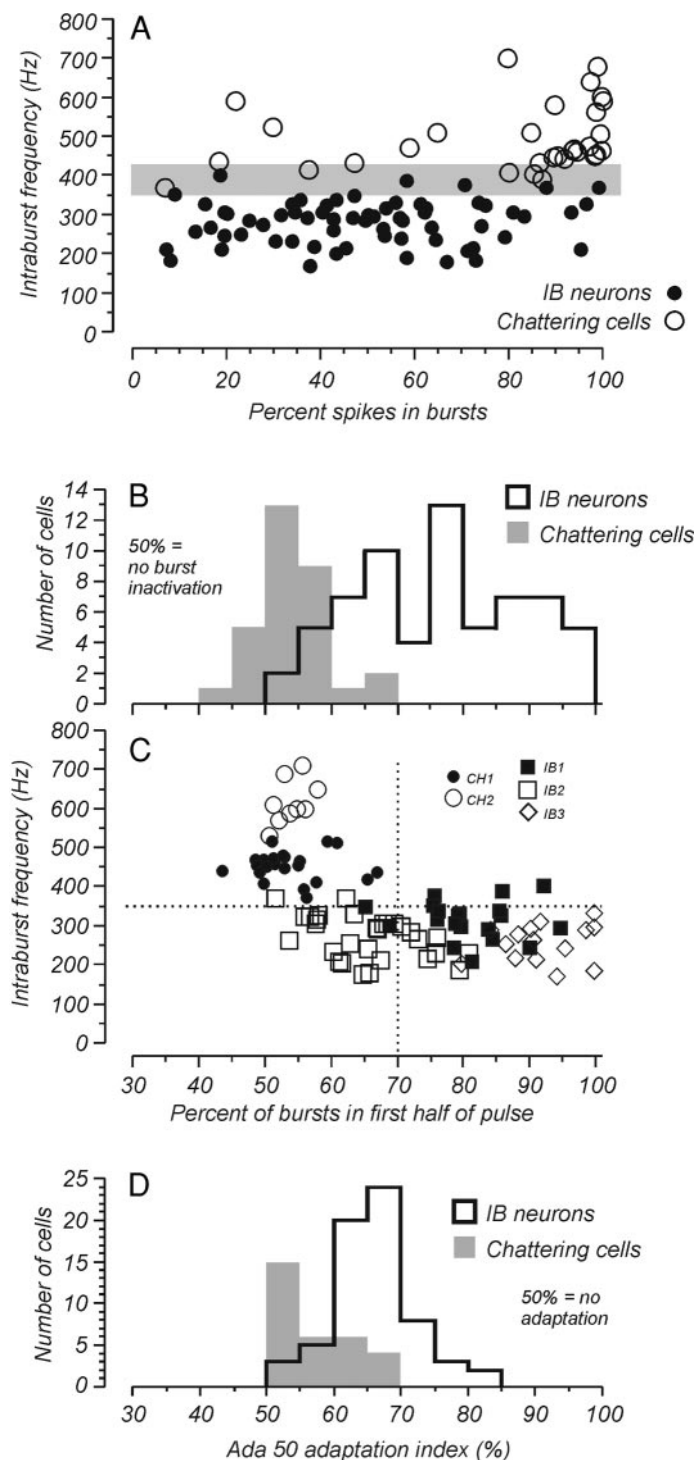


FIG. 10. Comparison of burst properties in CH and IB neurons. *A*: intraburst frequency plotted against percentage of spikes in bursts. Gray shading corresponds to the region of overlapping intraburst frequency for IB and CH neurons. *B*: histogram of burst inactivation indices in CH and IB cells. *C*: intraburst frequency and burst inactivation index plotted together. IB and CH cells could be accurately classified by these 2 criteria since all but 2 cells with an intraburst frequency >350 Hz and $<70\%$ of their bursts in the 1st half of the pulse appear to be CH neurons. Subclasses of neurons are also identified by different symbols to emphasize differences in burst inactivation between the 3 subtypes of IB cells and differences in intraburst frequency between the 2 subtypes of CH cells. *D*: adaptation of action potential firing in bursting neurons. Although there is substantial overlap, CH cells on average exhibit less adaptation than IB neurons.

Within the class of FS cells, cluster analysis also identified two subclasses of neurons that were distinct from each other (MANOVA, $P < 0.0001$). This difference was due mainly to the slope of their f - I relation (Fisher's PLSD, $P < 0.001$), while spike width or adaptation strength did not yield a significant difference ($P > 0.05$). Traditionally, FS neurons have steep f - I curves. The subclass of neurons having this property were therefore named "classical" FS neurons (FS_C), while the second subclass was termed FS_{LFI} (FS, less steep f - I).

CLUSTER ANALYSIS OF BURSTING NEURONS. Three variables, measured in bursting neurons, proved to be particularly useful in segregating neuronal subtypes. These included the intraburst firing rate, spike width, and the burst inactivation index (i.e., the ratio of the number of bursts occurring during the first half of the pulse to the number of bursts over the whole pulse duration; see METHODS). The dendrogram of the cluster analysis based on these three indices (Fig. 6*B*) revealed two main branches corresponding to the subjectively identified CH cells and IB neurons. The vast majority (94%) of the subjectively classified IB cells were found in the quantitatively established cluster of IB cells. They were characterized (on average) by relatively broad action potentials, lower intraburst firing rates, and pronounced burst inactivation during maintained depolarization. In the second class of bursting neurons, 73% of the subjectively classified CH cells were found in the quantitatively established cluster. These cells generated high-frequency bursts of relatively thin spikes, and displayed much less burst inactivation.

The addition of several other variables to the cluster analysis produced only small changes to the classification scheme. For example, including our measure of firing rate adaptation (i.e., "ada50" index; see METHODS and Fig. 4) also resulted in dendrograms with two main branches (data not shown) that separated at an aggregation distance of 68. This had the effect of adding four cells to the CH cluster while removing one. However, this manipulation also increased the heterogeneity of cell properties within clusters, and so we chose not to include this variable in the final classification of bursting neurons. Similarly, including the slope of the f - I relationship to the cluster analysis (data not shown) reduced the aggregation distance of the main branch and changed cluster membership for only two cells. In the newly formed CH cluster one cell came from the original IB cluster and one cell in the original CH cluster was moved to the new IB cluster. Finally, including the percentage of spikes occurring during bursts reduced the aggregation distance to 64 and moved six cells (all of which had a low percentage of spikes in bursts) from the CH class to the IB class (data not shown). Since including this variable had only a small effect on cluster membership, but produced a marked increase in the overlap of variable distributions, we also chose not to include it in the final cluster analysis (Fig. 6*B*). Thus the addition of either one or several of these variables to the three initially used changed the classification of only a small number of cells, indicating that the two main clusters are robust. Therefore for the remainder of this paper, the cells have been classified as IB or as CH on the basis of the cluster analysis using intraburst frequency, spike width, and burst inactivation properties only.

At aggregation distances between 10 and 20 (Fig. 6*B*), branching was observed that led to five statistically significant

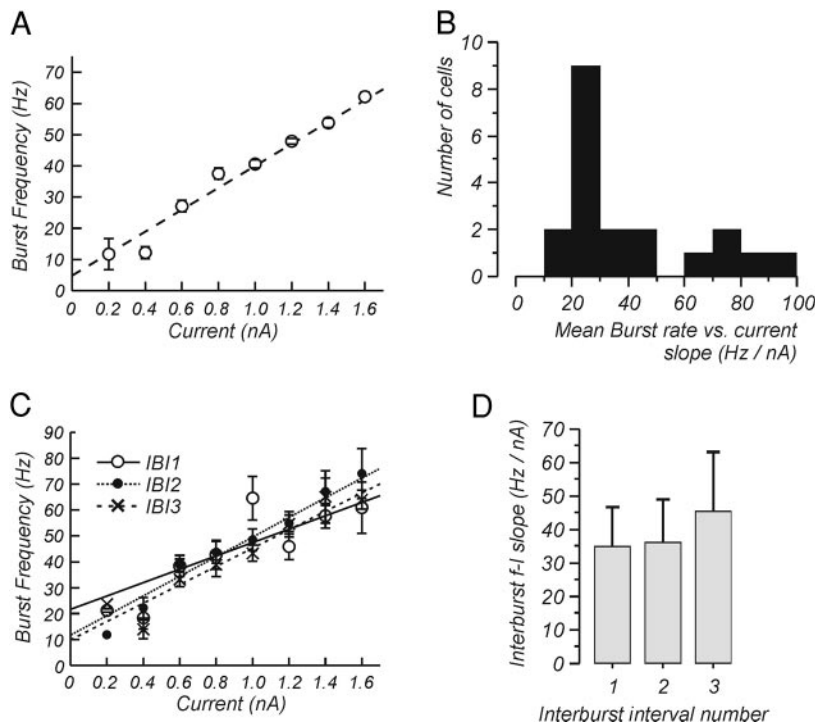


FIG. 11. Burst firing rate and adaptation of burst firing in chattering cells. *A*: example of the relationship between burst discharge rate and current intensity (same cell as Fig. 1C). Burst rate was averaged from multiple pulses of the same intensity. The slope for this cell was 35.1 Hz/nA. Bars represent SE. *B*: histogram of the slope of the relationship between current intensity and mean interburst frequency for 20 CH cells. *C*: relationship between current intensity and interburst frequency for the 1st 3 consecutive interburst intervals (IBI) for the same cell as in *A*. Bars represent SE. Slope values for IBI1, IBI2, and IBI3 were 25.8, 37.9, and 35.4 Hz/nA, respectively. *D*: population data for the slope of the relationship between current intensity and interburst frequency. Mean \pm SE values are presented for a sample of 7 CH cells.

subgroups—three for IB neurons and two for CH cells (MANOVA test, $P < 0.0001$). No single variable included in the cluster analysis cleanly distinguished between these subtypes of IB or CH neurons, although a combination of two parameters did. IB1 cells exhibited relatively thin spikes and higher intraburst firing rates, IB2 cells showed less burst inactivation and thin spikes, and IB3 neurons were characterized by broader spikes and higher burst inactivation. CH1 cells were distinguished from CH2 cells by a generally higher intraburst firing rate and shorter duration action potentials. Although statistically significant, the membership of these subclusters depended strongly on the variables included in the cluster

analysis. For example, inclusion of the slope of the f - I relationship also produced three subclusters of IB cells, but these subclusters were very different from those originally obtained.

To conclude this section, it appears that we can distinguish four main classes of neurons on the basis of electrophysiological criteria applied to our in vivo intracellular recordings. These four classes correspond well to the subjectively characterized RS, FS, IB, and CH classifications. Subclasses within each of these main classes could be also distinguished with cluster analysis. However, contrary to the main classes, these subclasses were strongly dependent on the particular variables included in the cluster analysis. For this reason, we have

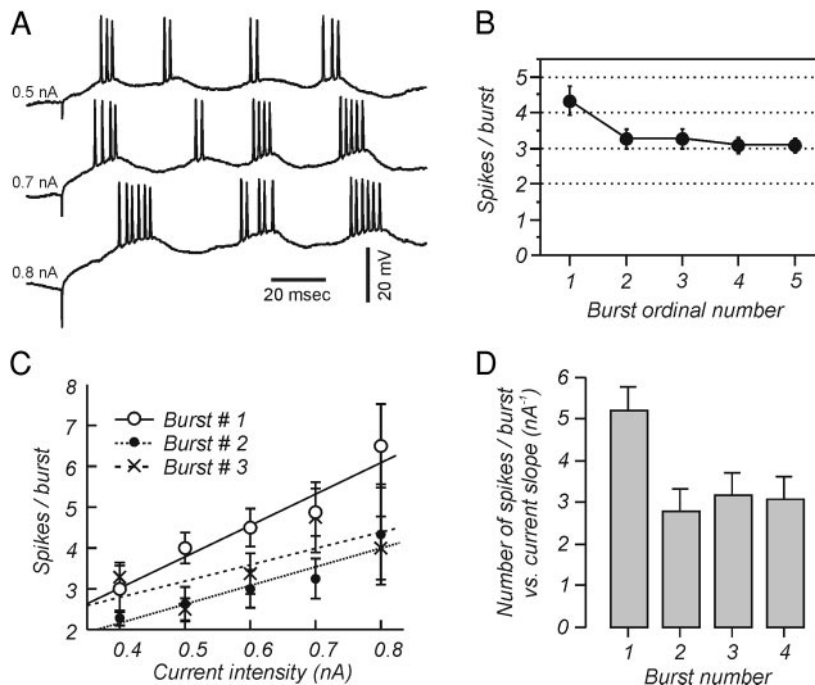


FIG. 12. Adaptation of the number of spikes per burst in chattering cells. *A*: traces represent burst discharge of a CH cell for 3 different current intensities. Two features of the burst discharge are illustrated in this example: 1st, for a given current intensity, the number of spikes in the first burst of the discharge is usually larger than in the subsequent bursts; 2nd, the number of spikes/burst increases when the current intensity is increased. *B*: plot of the mean (\pm SE) number of spikes per burst as a function of the burst ordinal number. All cells ($n = 25$) and current intensities have been averaged. The number of spikes per burst decreases with the ordinal number of the burst. *C*: in some CH cells, the number of spikes per burst increases in proportion to the current intensity. The graph corresponds to the cell illustrated in *A*. The number of spikes per burst, for the 1st, 2nd, and 3rd burst of the discharge, is represented as a function of current intensity. Responses to several current pulses of the same intensity have been averaged and the bars represent SE. *D*: population data: the mean (\pm SE) value of the slope of the relationship between number of spikes per burst and current intensity is represented for the 1st ($n = 18$ cells with significant relationship), 2nd ($n = 11$), 3rd ($n = 12$), and 4th ($n = 11$) burst of the discharge. The slope is significantly steeper for the 1st burst of the discharge compared with the 2nd, 3rd, and 4th.

TABLE 1. *Input resistance and time constant, main classes*

| | 1—Regular Spiking ($n = 33$) | 2—Fast Spiking ($n = 12$) | 3—Intrinsically Bursting ($n = 12$) | 4—Chattering ($n = 11$) |
|--------------------------------|--|---|--|--|
| Input resistance ($M\Omega$) | 51.3 ± 17.4 [20.7–90.8] ^{>4} | 41.7 ± 20.5 [13.2–79.1] | 39.2 ± 10.2 [22.9–53.6] | 37.8 ± 11.3 [23.5–58.9] ^{<1} |
| Time constant (ms) | 10.4 ± 3.5 [4.6–20.4] ^{>2} | 7.6 ± 4.2 [3.2–12.7] ^{<1,3} | 11.1 ± 2.3 [8.4–16.4] ^{>2} | 9.5 ± 4.7 [3.8–21.3] |

Values are mean \pm SD. Values between brackets: minimum and maximum. Sample size (n) lower than indicated in text because resistance and time constant have been measured on a subsample of cells. Numbers in exponent correspond to column numbers with which a statistically significant difference has been observed, and the $>$ or $<$ indicate the direction of the difference. For example, the input resistance in regular spiking neurons (column 1) is significantly larger than that in chattering cells (column 4) and this is indicated by “>4”.

concentrated our analysis on the four main classes of neuron (RS, IB, CH, FS), and mention only briefly the properties of the subclasses.

Electrophysiological properties

The cluster analysis revealed that of the 220 cells we analyzed, 91 (41.4%) were RS (54 RS_{TS} and 37 RS_C), 33 (15%) were FS (15 FS_C and 18 FS_{LFI}), 31 (14.1%) were CH (22 CH1 and 9 CH2), and 65 (29.5%) were IB (20 IB1, 30 IB2, and 15 IB3). Following this classification, we further analyzed the distributions of the electrophysiological properties of these cells. These distributions are illustrated in Figs. 7–12 and statistical summaries, together with an indication of significance of differences, can be found in Tables 1–8. Among these different properties, those that proved to be the most relevant for classification are spike width and adaptation index for FS and RS neurons, and intraburst firing rate, used together with either spike width or burst inactivation index, for CH and IB neurons.

INPUT RESISTANCE AND MEMBRANE TIME CONSTANT. The apparent input resistance was measured for a random subset of each physiological class of cells (Table 1) and was found to be significantly lower in CH cells compared with RS cells ($P = 0.02$, t -test). As far as subclasses are concerned, we found significantly different input resistance between the two subclasses of RS cells (Table 2), which was lower in RS_{TS} neurons compared with RS_C neurons ($P = 0.014$).

The mean membrane time constant (Table 1) was significantly shorter in FS neurons compared with both RS neurons ($P = 0.03$, t -test) and IB neurons ($P = 0.02$). This difference might result from the very short time constant exhibited by FS_C cells (Table 2), which is significantly shorter than that mea-

TABLE 2. *Input resistance and time constant, subclasses (values are given only when statistically significant differences were observed between subclasses of a given class)*

| Input Resistance ($M\Omega$) | |
|--------------------------------|-------------------------------|
| RS _C ($n = 16$) | RS _{TS} ($n = 17$) |
| 58.8 ± 17.7 [27.6–90.8] | 44.3 ± 14.3 [20.7–74.5] |
| Time Constant (ms) | |
| FS _{LFI} ($n = 8$) | FS _C ($n = 4$) |
| 9.4 ± 3.9 [3.8–12.7] | 3.8 ± 1.1 [3.2–5.5] |

Values are mean \pm SD. Between brackets: minimum and maximum values. Sample size (n) differs from values indicated in text as measurements have been made on a subsample of cells.

sured in FS_{LFI} cells ($P = 0.02$). No significant difference was observed between the membrane time constant of CH cells and that of the other cell classes.

ACTION POTENTIAL WIDTH AND MAXIMAL DEPOLARIZATION AND REPOLARIZATION RATES. Comparison of the action potential widths for the four classes of neurons revealed two distinct groups: both FS and CH cells exhibited short-duration action potentials, while IB and RS cells showed a broader distribution having, on average, more prolonged action potentials (Fig. 7A, Table 3). The average action potential width was not significantly different between IB and RS cells ($P = 0.75$, Fisher's PLSD). However, the distribution for RS cells was broader and included cells with short-duration action potentials, including the subclass RS_{TS} (Fig. 7A); approximately 15% of the RS cells (all members of the RS_{TS} subclass) displayed action potentials as thin as those of FS cells. The populations of bursting neurons also overlapped in their spike duration; the 50–100 percentile range for CH cells overlaps with the 0–25 percentile range for IB neurons (Fig. 7A). These results indicate that spike width alone cannot unambiguously discriminate one cell class from another in either the bursting or nonbursting categories.

The maximal rate of rise of the action potential (Table 3) was slightly larger (15–25%) for CH cells compared with FS ($P = 0.02$, t -test), RS ($P = 0.0002$), and IB neurons ($P = 0.04$), suggesting a higher sodium channel density for CH cells, a factor that might play a key role in the generation of bursting for these cells (Brumberg et al. 2000).

Compared with the rate of rise, however, we found a much larger difference between cell classes for the rate of fall. On average, this parameter was approximately two times greater for CH neurons and FS cells compared with RS and IB cells (Table 3; $P < 0.0001$ in all 4 comparisons). These results indicate that the short-duration of action potentials in FS and CH neurons is mostly due to a faster action potential repolarization.

Previously, the ratio of maximal rate of rise to maximal rate of fall of the action potential has been used to distinguish between FS and RS neurons (McCormick et al. 1985). We also measured this ratio and found there are two groups of distributions, with CH and FS neurons on the one hand and IB and RS neurons on the other hand, exhibiting similar ratios (Fig. 7B and Table 3). Within these two subdivisions, the ratios for the different cell classes were statistically indistinguishable. These ratios were significantly larger in FS and CH neurons compared with IB and RS neurons ($P < 0.0001$ all comparisons).

Finally, we found that action potential parameters also distinguished between subclasses of cells. The RS_{TS} subclass contained cells with spikes that were significantly shorter than

TABLE 3. Action potential features, main classes

| | 1—Regular Spiking (n = 91) | 2—Fast Spiking (n = 33) | 3—Intrinsically Bursting (n = 65) | 4—Chattering (n = 31) |
|---|--|--|--|--|
| Action potential width at half height (ms) | 0.61 ± 0.22 [0.18–1.33] ^{>2,4} | 0.28 ± 0.08 [0.16–0.48] ^{<1,3} | 0.60 ± 0.15 [0.28–0.96] ^{>2,4} | 0.31 ± 0.10 [0.14–0.50] ^{<1,3} |
| Action potential maximal rate of rise (V/s) | 345 ± 103 [155–700] ^{<4} | 360 ± 122 [174–701] ^{<4} | 381 ± 110 [202–731] ^{<4} | 436 ± 140 [251–749] ^{>1,2,3} |
| Action potential maximal rate of fall (V/s) | 124 ± 61 [33–358] ^{<2,4} | 214 ± 72 [101–389] ^{>1,3,<4} | 127 ± 41 [57–282] ^{<2,4} | 268 ± 119 [123–606] ^{>1,2,3} |
| Ratio of rate of rise/rate of fall | 0.366 ± 0.142 [0.154–0.836] ^{<2,4} | 0.603 ± 0.106 [0.399–0.838] ^{>1,3} | 0.347 ± 0.114 [0.152–0.697] ^{<2,4} | 0.606 ± 0.123 [0.350–0.828] ^{>1,3} |

Values are mean ± SD and [minimum–maximum]. > and < signs and numbers that follow refer to columns with statistically significant differences.

TABLE 4. Action potential features, subclasses (values are given only when statistically significant differences were observed between subclasses within a given class)

| | Action Potential Width at Half Height (ms) | Action Potential Maximal Rate of Fall (V/s) | Ratio of Rate of Rise/Rate of Fall |
|---------------------------|--|---|------------------------------------|
| RS _C (n = 37) | 0.77 ± 0.19 [0.56–1.33] | 89 ± 25 [33–145] | 0.269 ± 0.060 [0.154–0.377] |
| RS _{TS} (n = 54) | 0.50 ± 0.16 [0.18–0.80] | 148 ± 67 [64–358] | 0.433 ± 0.145 [0.180–0.836] |
| CH ₁ (n = 22) | 0.34 ± 0.10 [0.17–0.50] | — | 0.574 ± 0.109 [0.350–0.732] |
| CH ₂ (n = 9) | 0.25 ± 0.06 [0.14–0.32] | — | 0.686 ± 0.125 [0.458–0.828] |
| IB ₁ (n = 20) | 0.44 ± 0.07 [0.28–0.56] | 155 ± 41 [99–282] | 0.416 ± 0.096 [0.289–0.619] |
| IB ₂ (n = 30) | 0.64 ± 0.10 [0.49–0.96] | 123 ± 37 [57–214] | 0.346 ± 0.113 [0.191–0.697] |
| IB ₃ (n = 15) | 0.75 ± 0.12 [0.54–0.92] | 99 ± 26 [65–146] | 0.257 ± 0.069 [0.152–0.364] |

Values are mean ± SD and [minimum–maximum].

TABLE 5. Firing rate and ada50 index, main classes

| | 1—Regular Spiking | 2—Fast Spiking | 3—Intrinsically Bursting | 4—Chattering |
|----------------------------|---|---|---|---|
| <i>f</i> -I slope (Hz/nA) | 135 ± 67 [45–375] ^{<2,4} | 351 ± 157 [106–783] ^{>1,3,4} (FS _{LFI} : 234 ± 57 [106–349]) (FS _C : 492 ± 114 [356–783]) | 128 ± 74 [41–369] ^{<2,4} | 180 ± 105 [55–436] ^{<2,>1,3} |
| Ada50 adaptation index (%) | 59.9 ± 5.9 [41.3–73.3] ^{>2,4,<3} | 50.0 ± 3.8 [39.1–57.9] ^{>1,3,4} | 65.6 ± 6.2 [50.0–80.2] ^{>1,2,4} | 55.8 ± 6.1 [50.0–69.9] ^{>2,<1,3} |

Values are mean ± SD and [minimum–maximum]. Numbers preceded by > and < sign refer to column number with statistically significant differences and to the direction of the difference. The *f*-I slope values are also given separately for FS_{LFI} and FS_C cells in the fast spiking cells column as these two subclasses of fast spiking cells showed a significant difference for this variable.

TABLE 6. Adaptation parameters in regular spiking and fast spiking cells

| | Regular Spiking | Fast Spiking |
|--|--|---|
| Adaptation index (%)* | 56.4 ± 13.2 [21.6–84.1] (RS _C : 68.7 ± 6.6 [55.0–84.1]) (RS _{TS} : 47.9 ± 9.3 [21.6–68.0]) | 9.1 ± 14.3 [–26.9–32.1] |
| Slope of <i>f</i> -I for first interspike interval (Hz/nA) | 357 ± 180 [84–937] | 408 ± 191 [119–1020] (FS _{LFI} : 291 ± 100 [119–471]) (FS _C : 548 ± 182 [303–1020]) |
| Adaptation time constant (ms)* | 21.6 ± 14.5 [3.9–65.4] (n = 83) | 9.9 ± 9.9 [1.4–33.4] (n = 16) |

Values are means ± SD. Between brackets: minimum and maximum. Sample size (n) given for adaptation time constant since it could not be measured in all the cells. * Regular spiking and fast spiking cells showed statistically significant differences for adaptation index and adaptation time constant but not for the *f*-I slope of the first interspike interval of the current evoked discharge. The adaptation index values are also given for RS_{TS} and RS_C subclasses since these showed a significant difference for this variable. Likewise for the slope of the *f*-I slope of the first interspike interval for FS_{LFI} and FS_C cells.

TABLE 7. Parameters characterizing bursts and burst discharge in burst-generating neurons, main classes

| | Intrinsically Bursting | Chattering |
|---------------------------|-------------------------|-------------------------|
| Percent spikes in burst* | 49.3 ± 23.7 [7.1–99.1] | 78.0 ± 27.8 [6.8–99.9] |
| Number of spikes/burst | 2.78 ± 0.56 [2.00–5.87] | 3.06 ± 1.36 [2.00–8.32] |
| Intraburst frequency* | 281 ± 56 [170–402] | 495 ± 85 [369–701] |
| Burst inactivation index* | 76.3 ± 12.9 [51.5–100] | 53.9 ± 4.9 [43.6–66.9] |

Values are means ± SD and [minimum–maximum]. * Statistically significant differences are observed between IB and CH cells for the percentage of spikes in burst, the intraburst frequency and the burst inactivation index (percent of bursts that are in the first one-half of the pulses) but not for the number of spikes per burst.

the RS_C subclass (Table 4; $P < 0.0001$, Fisher's PLSD test). Spike width and the ratio of the rate of rise to the rate of fall also differed significantly between subclasses (Table 4) of both CH ($P = 0.015$) and IB cells ($P < 0.001$).

FIRING RATE VERSUS INJECTED CURRENT. The distribution of the slopes of the f - I relationship revealed that FS cells are substantially different from the other three cell classes in this regard (Fig. 7C; Table 5); the median slope values for FS cells were 1.7 times larger than for CH cells, 2.3 times larger than for RS cells, and 2.7 times larger than for IB cells ($P < 0.0001$ in the 3 comparisons, Fisher's PLSD). In addition, CH cells exhibited a slightly steeper slope than RS and IB cells (Fig. 7C; Table 5; $P = 0.01$ and $P = 0.02$ for CH cells vs. IB and RS neurons, respectively).

Only within the FS class did subclasses of cells differ significantly ($P < 0.0001$) with respect to the slope of the f - I relationship (Table 5; Fig. 8A), with FS_C cells displaying a steeper slope than FS_{LFI} cells.

When spike widths and f - I slopes are represented together (Fig. 8A), it appears that all the cells with action potential widths briefer than 0.5 ms and f - I slopes larger than 300 Hz/nA are FS. Irrespective of slope value, all the cells with action potential width larger than 0.5 ms have been classified as RS. However, there are a large number of FS cells that cannot be differentiated from RS cells based on action potential width and f - I slope alone (spike width <0.5 ms and f - I slope <300 Hz/nA; Fig. 8A).

ADAPTATION PROPERTIES OF FAST SPIKING AND REGULAR SPIKING NEURONS. One additional feature that was able to distinguish between RS and FS neurons was their degree of adaptation (Fig. 8B; Table 6). RS neurons adapted their firing rates by an average of 56.3% while FS neurons adapted by only 9.1%. Eight FS cells even possessed an adaptation index that

was negative (i.e., their firing rates increased during the current pulse). The distribution of adaptation indices for RS and FS cells shows only a limited overlap, restricted to values between 20% and 35%.

When adaptation index was combined with action potential width, it was possible to accurately distinguish between FS and RS cells (Fig. 8C). Neurons that had a spike width <0.5 ms and an adaptation index lower than 35% were almost always (except for 3 RS cells) clustered as FS neurons.

Figure 8C also shows that RS cells with thin spikes (RS_{TS}) adapt significantly less ($P < 0.0001$, Fisher's PLSD test) than RS cells with broad spikes (RS_C; Table 6). Combining adaptation index and spike width also gave a good segregation between these two subtypes of RS cells.

Figure 8D illustrates the distribution of adaptation time constant for RS neurons as well as for some FS neurons. This variable could not be measured in all the cases, due to the lack of adaptation or to poor fitting for 17 of 33 FS cells and 8 of 91 RS cells. Since the adaptation time constant could not be determined for all the cells, it was not used for the cluster analysis presented in Fig. 6. Nevertheless, a strong difference appeared between the FS and RS cells, which adapted with time constants of $9.9 ± 9.9$ ms (median: 5.4 ms) and $21.6 ± 14.5$ ms (median: 17.4 ms), respectively. Within both the RS and FS classes, the subclasses did not show significant differences in terms of adaptation time constant.

Considering adaptation index and time constant together (Fig. 8E), the FS cells showed much less adaptation than the RS cells, although many of them adapted at the same rate.

BURST CHARACTERISTICS IN INTRINSICALLY BURSTING AND CHATTERING CELLS. Cluster analysis revealed two main classes of bursting cells, the IB and CH neurons. IB cells did not differ from CH cells in the mean number of spikes per burst (Table 7; $P = 0.16$, t -test), but the average intraburst frequency (Table 7) was higher in CH cells ($496 ± 85$ Hz) than in IB neurons ($281 ± 56$ Hz; $P < 0.0001$). Although the distribution of intraburst frequencies showed some overlap between these two cell types (Fig. 9B), it was limited to a narrow range of values (350–425 Hz). Thus based on this criterion alone, a significant degree of segregation could be achieved as 84% of the CH cells displayed an intraburst frequency >425 Hz and 89% of the IB neurons showed an intraburst frequency <350 Hz.

Intraburst frequency also differed significantly between the CH1 and CH2 subclasses ($P < 0.0001$) with CH2 cells showing the highest intraburst firing rates (Table 8; Fig. 9C). Differences in intraburst frequency were not significant between IB2 and IB3 subtypes of IB cells, but were significant between IB1 and IB2 subtypes ($P = 0.004$) and between IB1 and IB3

TABLE 8. Burst and adaptation related variables characterizing subclasses of burst-generating neurons (values are given only when statistically significant differences were observed between subclasses of a given class)

| | Intraburst Frequency (Hz) | Burst Inactivation Index (%) | Proportion of Spikes in Burst (%) | Ada50 (%) |
|------------------------------|---------------------------|------------------------------|-----------------------------------|------------------------|
| CH ₁ ($n = 22$) | 449 ± 37 [369–511] | — | — | — |
| CH ₂ ($n = 9$) | 609 ± 56 [526–701] | — | — | — |
| IB ₁ ($n = 20$) | 316 ± 49 [212–402] | 80.7 ± 7.2 [65.1–94.4] | 37.7 ± 19.9 [7.1–73.5] | 62.0 ± 6.1 [50–75.7] |
| IB ₂ ($n = 30$) | 273 ± 53 [181–369] | 65.6 ± 7.6 [51.5–80.8] | 63.2 ± 22.1 [13.2–99.1] | 66.8 ± 5.8 [56.8–80.2] |
| IB ₃ ($n = 15$) | 253 ± 48 [170–328] | 92.0 ± 6.1 [79.8–100.0] | 37.1 ± 16.0 [7.8–61.2] | 68.1 ± 5.2 [60.7–80.2] |

Values are means ± SD and [minimum–maximum].

neurons ($P = 0.0005$). IB1 cells showed the highest intraburst frequency (Table 8; Fig. 9C).

Intraburst frequency and action potential width covaried in CH and IB cells, although with different slopes (Fig. 9, A and C). Using these two parameters enabled a nearly complete separation of CH and IB cells (Fig. 9C), because cells that exhibited an intraburst frequency of >350 Hz and action potential widths of ≤ 0.5 ms were almost always (except for 2 IB cells, representing 3% of the IB cells) clustered as CH neurons.

BURSTS AND SINGLE SPIKE DISCHARGES. Only a small minority of bursting cells generated 100% of their action potentials in bursts (Figs. 4E and 10A; Table 7). This percentage was highest for CH cells, with more than two-thirds (12/31) of these cells generating $>80\%$ of their spikes in bursts (Fig. 10A; Table 7). In contrast, IB neurons exhibited a uniformly broad distribution for the percentage of spikes occurring during bursts. Despite these differences, the broad overlap of these two populations did not permit this parameter to distinguish unambiguously between CH and IB neurons (Fig. 10A). Moreover, combining the intraburst frequency with the percentage of spikes in bursts did not allow a clean separation between the CH and IB cell types, because of the relatively continuous overlap among those cells having intraburst frequencies between 350 and 425 Hz (Fig. 10A).

Significant differences between IB1 and IB2 ($P < 0.0001$), and IB2 and IB3 ($P = 0.0001$) subclasses were apparent, however, with IB2 cells exhibiting a larger proportion of spikes within bursts (Table 8) compared with the other two subtypes, which did not differ significantly in this respect ($P = 0.93$).

BURST INACTIVATION. Although some IB neurons are able to burst repetitively in response to sustained current injection (Agmon and Connors 1989; Dégenétais et al. 2002; Silva et al. 1991; Steriade et al. 2001), these cells usually generate a burst of action potentials only at the beginning of the current pulse (e.g., Connors et al. 1982; McCormick et al. 1985). On the other hand, CH cells typically generate bursts throughout the duration of a maintained depolarization (Brumberg et al. 2000; Gray and McCormick 1996; Steriade et al. 1998). Here we examined this feature quantitatively using the burst inactivation index (i.e., the percentage of bursts in the first half of the current pulse relative to the total number of bursts, with 50% indicating an equal number of bursts in the first and second halves of the current pulse). On average, CH cells generated $53.9 \pm 4.9\%$ of their bursts in the first half of the pulse, indicating that they tend to generate bursts throughout the duration of the depolarization. IB neurons had $76.3 \pm 12.9\%$ of their bursts in the first half of the pulse, indicating that these cells are much less likely to repetitively burst during maintained depolarization ($P < 0.0001$, Fisher's PLSD). However, the distribution of burst inactivation indices showed some overlap between CH and IB neurons (Table 7; Fig. 10B). This indicates that some repetitively bursting cells could be quantitatively classified as IB neurons (for example the cell in Fig. 2F). These were mostly found in the IB2 subclass, where neurons showed the lowest burst inactivation index (Table 8; Fig. 10C). All three subclasses of IB cells differed significantly with respect to this variable ($P < 0.0001$ for the all comparisons).

All parameters taken into account, IB1 and IB3 cells appear

similar to classic IB neurons, in that they generate a burst of spikes at the beginning of the current pulse, but tend to convert to single spike activity thereafter. The main difference between IB1 and IB3 cells is in spike width: IB1 neurons generate action potentials of shorter duration. IB2 cells appear to correspond to a population of repetitively bursting IB neurons, also displaying a high proportion of spikes in bursts which is related to the low inactivation of burst firing.

Plotting the percent of bursts in the first half of the current pulse versus the intraburst firing rate revealed a good segregation of CH and IB neurons. All CH cells had intraburst firing rates >350 Hz and $<70\%$ of their bursts occurred in the first half of the pulse (Fig. 10C). Together, these two variables correctly identified all CH cells and all but two (3%) IB neurons.

ADAPTATION OF SPIKE DISCHARGE IN BURST-GENERATING NEURONS. Spike frequency adaptation could not be examined as thoroughly in bursting neurons as in nonbursting cells due to the intermixing of single spikes and burst discharges. Our measure of adaptation strength for bursting cells was the proportion of spikes in the first 50 ms of the current pulses relative to the number of spikes present during the first 100 ms ("Ada50" index). Although the distribution of values showed some overlap (Table 5; Fig. 10D), the ada50 index was significantly smaller for CH cells ($P < 0.0001$, *t*-test) compared with IB neurons. This indicates that adaptation of spike discharge was quite low for CH cells, although on average it differed significantly from 50% (1 sample *t*-test, $P < 0.0001$). This value is also significantly smaller ($P = 0.001$) than the ada50 index displayed by RS cells (Table 5), but larger than that shown by FS cells ($P < 0.0001$).

There was no significant correlation between adaptation and burst inactivation in CH cells ($P = 0.2$) or in IB neurons ($P = 0.16$). This indicates that the adaptation of action potential firing is not simply a consequence of the cessation of bursting during the current pulse.

Within the IB cell class, the IB1 subtype displayed spike discharge adaptation that was significantly lower than for the two other IB subtypes (Table 8). Therefore in similarity with RS cells, the IB neurons with the shortest duration action potentials appear to adapt the least.

RHYTHMIC BURST DISCHARGE FREQUENCY IN CHATTERING CELLS. One of the defining features of CH cells is their ability to generate rhythmic bursts of action potentials at frequencies of 10–70 Hz (Gray and McCormick 1996). This was quantitatively explored at several current intensities in CH cells that repetitively burst without intervening isolated spikes.

The frequency of repetitive bursting depended strongly on the intensity of current injected and the relationship was relatively linear (1 example is shown in Fig. 11A). At the population level (Fig. 11B), the slope of the rhythmic burst frequency versus injected current was highly variable from cell to cell, with a mean value of 41.0 ± 24.5 Hz/nA ($n = 20$). This suggests that it would take an average of 1.15 nA (calculated from the fitted linear regression and taking into account offset) to generate rhythmic burst firing at 40 Hz in CH neurons in vivo.

We next examined the adaptation of rhythmic bursting in CH cells. Plotting the burst frequency versus injected current for the first, second, and third interburst intervals (IBI) revealed

a similar slope for all three (Fig. 11C, same cell as Fig. 11A), indicating a relative lack of adaptation of rhythmic bursting.

For seven cells, the relationship between current intensity and interburst frequency was significant for the first, second, and third interburst intervals. The slopes of the corresponding linear fits were very similar for the first and second interburst interval (34.9 ± 31.2 and 36.1 ± 34.0 Hz/nA; $P = 0.7$, paired t -test; Fig. 11D), while the third interval showed a steeper, but not significantly different ($P = 0.19$), slope (45.5 ± 47.0 Hz/nA, Fig. 11D). These results indicate that no adaptation of burst frequency discharge was observed in CH cells. Instead, a trend toward an acceleration of burst discharge was observed, although it was not significant (but see Brumberg et al. 2000).

ADAPTATION OF THE NUMBER OF SPIKES PER BURST IN CHATTERING CELLS. Although CH cells did not show adaptation of bursting rate during a current pulse, some degree of adaptation was found to take place in the number of action potentials generated within each burst (Fig. 12, A and B). On average ($n = 25$ cells with repetitive burst discharge without intervening single spikes for at least 1 current intensity), the first burst in CH cells contained 1.3 times the number of action potentials of the second burst and 1.4 times the number of action potentials of the fifth burst (Fig. 12B). Thus even though CH cells may not exhibit burst frequency adaptation (Fig. 11), the reduction in number of spikes per burst may result in an overall, although small, adaptation in average firing rate (Fig. 10D).

Another feature of the burst discharge in some (but not all) CH cells was an increase in the number of spikes per burst as a function of injected current (Fig. 12C). The slope of the linear fit to these data decreased with the ordinal position of the burst. The mean slopes for these relationships were 5.2 ± 2.3 spikes per burst per nA for the first burst ($n = 18$ cells), 2.8 ± 1.9 for the second burst ($n = 11$), 3.2 ± 1.8 for the third burst ($n = 12$), and 3.1 ± 1.8 ($n = 12$) for the fourth burst (Fig. 12D). The slope was significantly steeper for the first burst compared with the second, third, and fourth (paired t -test, $P = 0.005$, 0.002 , and 0.002 , respectively), while slopes for second, third, and fourth bursts did not differ significantly. This has the consequence that, with increasing intensity of current injection, adaptation of the number of spikes per burst is enhanced, since the first burst gains action potentials faster than subsequent bursts.

Morphological features, cortical layer distribution, and receptive field properties

MORPHOLOGICAL FEATURES OF ELECTROPHYSIOLOGICALLY DEFINED CELL CLASSES. Forty-eight cells (20 RS, 5 FS, 14 IB, and 9 CH) were filled with biocytin to an extent that allowed their somatic and dendritic morphology to be examined. Here we present the general characteristics and laminar location of these labeled neurons. Our sample size was too small to reach definitive conclusions regarding anatomical differences between the various subclasses.

Fast spiking neurons were multipolar aspiny or sparsely spiny nonpyramidal cells in layer 4 ($n = 4$, 1 FS_{LFI} and 3 FS_C cells) and layer 2/3 ($n = 1$ FS_C cell; data not shown). We have previously reported on the morphological and visual response properties of some of these neurons (Azouz et al. 1997). Three of the FS neurons appeared similar to basket cells (e.g., Martin

et al. 1983) and two were similar to small basket cells (e.g., "clutch" cells; Kisvárdy et al. 1985). Axonal projections of the basket cells were both local and horizontal, ≤ 0.5 –1 mm from the parent soma.

Regular spiking neurons were spiny pyramidal cells in layers 2 and 3 ($n = 7$; 37% of labeled layer 2–3 neurons), layer 5 ($n = 1$; 12.5% of labeled layer 5 neurons), and layer 6 ($n = 10$; 71% of labeled layer 6 neurons) as well as spiny stellate cells in layer 4 ($n = 2$). As might be expected, given that they were observed in all cortical layers, the RS category was morphologically diverse. RS cells in layer 2/3 (Fig. 13A) displayed horizontal axon collaterals in both supragranular and infragranular layers. Two RS cells in layer 4 displayed spiny stellate morphologies (Fig. 13B), while RS cells in layer 6 displayed a wide variety of morphologies. Five of these showed features of "corticothalamic type 1 neurons," as described by Katz (1987), with extensive dendritic and axonal arborization in layer 4 (Fig. 13C). Some layer 6 RS cells appeared to be pyramidal cells with small cell bodies, and one RS cell, located at the bottom of layer 6, appeared similar to a spiny stellate cell. Its dendrites were all of similar length and it lacked an obvious apical dendrite.

Among the 20 labeled RS cells, 7 belonged to the classical (RS_C) subclass and 13 to the thin spike (RS_{TS}) subclass. Both subtypes were found in multiple layers: supragranular layers contained 3 RS_C and 4 RS_{TS} neurons, layer 4 contained one of each subclass, and the infragranular layers had 3 RS_C and 8 RS_{TS} neurons.

Ahmed et al. (1998) found that RS cells located in the upper cortical layers of cat area 17 tend to display faster and stronger spike adaptation compared with those of the infragranular layers. While we observed a similar tendency, this was not found to be significant in our sample. Adaptation strength in supragranular layers averaged 60%, while it was 54% in infragranular layers ($P = 0.4$). Adaptation time constant in supragranular layers averaged 20 ms, while it was 28 ms in infragranular layers ($P = 0.3$).

CH neurons ($n = 9$) were found to be spiny pyramidal cells in layers 2/3 ($n = 8$, representing 42% of the labeled cells in layers 2/3 and corresponding to 6 CH1 and 2 CH2 cells) and spiny stellate cells in layer 4 ($n = 1$ of the CH1 subtype). Curiously, 7 of 8 of the supragranular CH cells were confined to the lower half of layers 2/3. CH cells with pyramidal morphology exhibited apical dendrites that ramified in layer 1 as well as basal dendrites in layers 2/3 (Fig. 14, A and B). Quite often the basal dendrites also extended into layer 4 (Fig. 14B). Although CH cells seem to be concentrated in a narrow band, their morphology can be quite variable from one cell to another; for example, the two cells in Fig. 14 are quite distinct in terms of number of basal dendrites. All of the CH cells that were well labeled exhibited an axon that entered into the white matter, indicating that these are projection neurons. Horizontal axon collaterals were observed in well filled CH cells ($n = 5$), both within layers 2/3 as well as within layer 5. These axon collaterals could travel for distances of several millimeters in layer 2/3. However, these morphological features were not restricted to CH cells, because they were also observed for RS cells in the supragranular layers ($n = 5$).

IB cells were found in layers 2/3 ($n = 3$; 16% of labeled layer 2/3 neurons), in layer 5 ($n = 7$; 87.5% of labeled layer 5

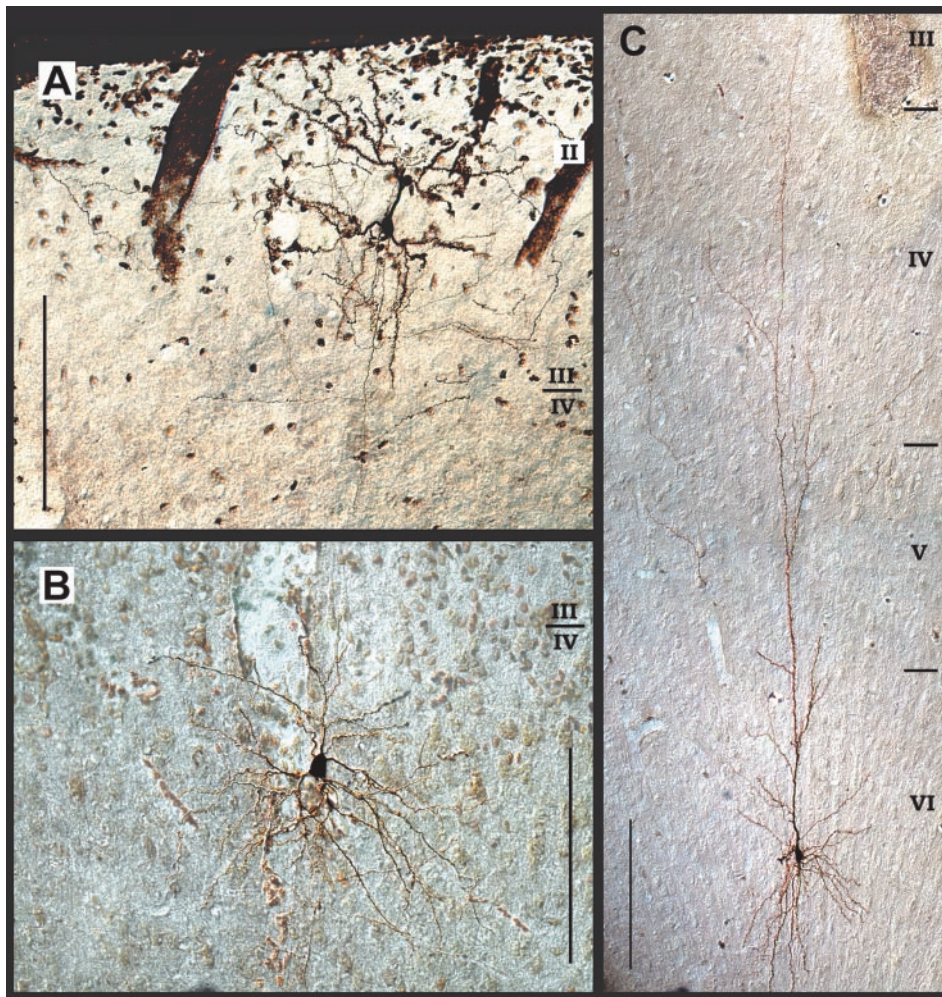


FIG. 13. Morphological features of electro-physiologically identified regular spiking cells. *A*: RS spiny pyramidal cell in layer 2/3. Note local horizontal collaterals leaving the main axon. *B*: RS spiny stellate cell from layer 4. Photomontage from 2 different sections. *C*: RS layer 6 pyramidal cell. Note dendritic and axonal arborization in layer 4, typical of "type 1" (Katz 1987) corticothalamic neurons. Scale bar in *A*–*C*: 200 μ m.

cells), and in layer 6 ($n = 4$; 29% of labeled layer 6 neurons). Similar to those recorded *in vitro*, IB neurons located in layer 5 exhibited large apical dendrites extending into layer 1, where they ramified extensively (Fig. 15A). These cells exhibited spiny apical and basal dendrites and that axonal projections

extended horizontally in layers 5 and 6 ($n = 5$; data not shown).

Some IB neurons of layer 6 exhibited morphological features similar to "type 1" corticothalamic neurons as described by Katz (1987), with an apical dendrite and axon collaterals

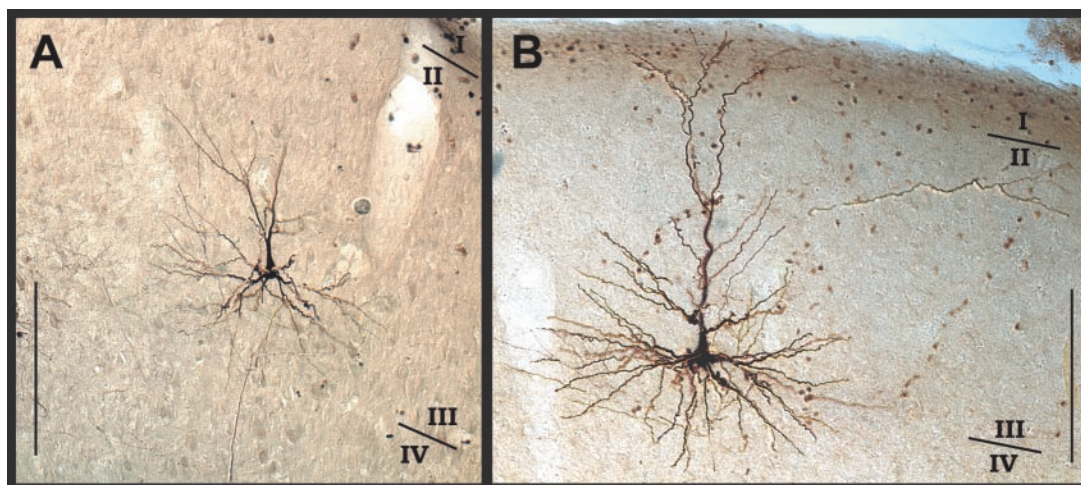


FIG. 14. Morphological features of chattering cells. Both *A* and *B* are photomontages from 2 different sections. Both cells are spiny pyramidal cells in the lower half of layers 2/3 and exhibit local axon collaterals as well as an axonal projection that enters the white matter (data not shown). Scale bar in *A* and *B*: 200 μ m.

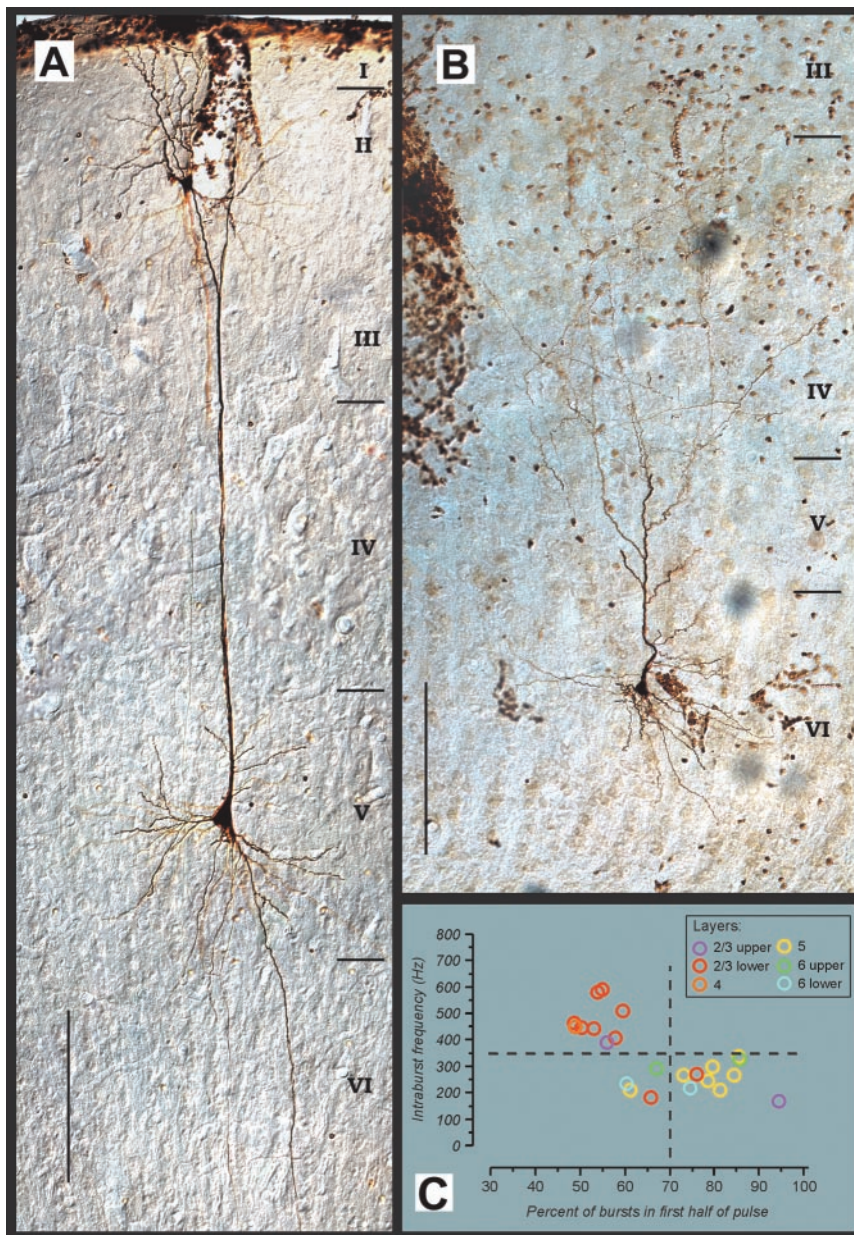


FIG. 15. Morphological features of IB neurons. *A*: IB pyramidal neuron in layer 5, exhibiting the typical feature of corticotectal neurons. *B*: IB pyramidal neuron in layer 6, with morphology similar to that of “type 1” (Katz 1987) corticothalamic neurons, including dendritic arborization and axon collaterals in layer 4. Scale bar in *A* and *B*: 200 μ m. *Bottom right* illustrates a plot of intraburst frequency as a function of burst inactivation index for CH and IB cells that have been labeled in this study. Note discharge features characteristic of CH cells in layer 4 and supragranular layers but not in infragranular layers.

arborizing abundantly inside layer 4 (Fig. 15*B*). However, RS cells with similar features were also observed (Fig. 13*C*); thus we were unable to distinguish between RS and IB neurons of layer 6 on the basis of their morphological features.

The distribution of IB neurons according to subclass was suggestive of a partial segregation for these neurons. Most (5/6) IB1 neurons (burst inactivating) were found in layer 5 (1 was located in the upper part of layer 6). In contrast, the distribution of IB2 neurons (repetitively bursting) suggests that they may be more evenly distributed across the cortical layers. Two of these cells were located in layer 2–3, two were in layer 5, and three were located in layer 6. Only one IB3 neuron was labeled and recovered histologically, and it was located in layer 2/3.

The two electrophysiological features that best identified the difference between CH and IB neurons (Fig. 10*B*) are shown in Fig. 15*C* with respect to the different cortical layers. This

shows that neurons with properties typical of CH cells (intra-burst frequency larger than 350 Hz and burst inactivation index lower than 70%) were found only in layers 2/3 and 4, whereas neurons with the electrophysiological signature of IB neurons were found in both supra- and infragranular layers, although in larger proportion in the latter.

RECEPTIVE FIELD PROPERTIES OF PHYSIOLOGICALLY DEFINED CELL CLASSES. Receptive field properties appeared to be more strongly constrained by the cortical layers than by either the morphological or electrophysiological subtypes. Most of the CH cells displayed simple receptive fields (11/12) and RS cells were either simple ($n = 24$) or complex ($n = 9$). When both receptive field type and laminar position were available, we observed the following: RS cells located in the supragranular layers could be either simple ($n = 3$) or complex ($n = 1$); one spiny stellate cell in layer 4 was found to be simple; and five of seven RS cells in layer 6 were found to possess simple

receptive fields. No RS cell with a characterized receptive field type was recovered in layer 5.

FS cells were both simple ($n = 6$) or complex ($n = 2$). Among the FS cells that were characterized functionally and morphologically ($n = 2$, both FS_C in layer 4), one located at the bottom of layer 4 displayed a complex receptive field. While spiny stellate cells located in layer 4 of cat area 17 all display simple receptive fields (Gilbert and Wiesel 1979; Martin and Whitteridge 1984), the presence of putative interneurons with complex receptive fields in layer 4 has already been documented in other studies (Ahmed et al. 1997; Hirsch et al. 2000; Martin et al. 1983).

Most of the IB neurons were found to be complex ($n = 9$ complex vs. 3 simple IB cells). This is likely to be related to their prevalence in layer 5, where most cells display complex receptive fields (Bullier and Henry 1979; Gilbert 1977; Gilbert and Wiesel 1979; Leventhal and Hirsch 1978; Martin and Whitteridge 1984). Thus all labeled IB neurons located in layer 5 had complex receptive fields ($n = 5$, corresponding to 3 IB1 and 2 IB2 cells). In layer 6, however, 1 labeled IB neuron was simple while another one was complex.

DISCUSSION

In an effort to understand the basic circuitry and operation of the cerebral cortex, physiological studies have repeatedly attempted to identify unique categories of neurons that occupy distinct anatomical and functional positions. The identification of unique physiological cell classes, however, has several inherent difficulties, including the subjective nature of most classification schemes and the lack of statistical demonstration that newly defined groups actually represent distinct classes. Here we have used quantitative methods to demonstrate the existence of distinct physiological classes of neurons in the adult cat primary visual cortex *in vivo*. The four major classes quantitatively demonstrated closely matched the subjectively defined regular spiking (RS), fast spiking (FS), intrinsically bursting (IB), and chattering (CH) categories (Connors et al. 1982; Gray and McCormick 1996; McCormick et al. 1985). Our results therefore confirm the prior contention that these four classes represent distinct physiologically defined subtypes of cortical neurons. Cluster analysis also indicated that each of these main categories are themselves composed of distinct subclasses, each displaying a unique combination of spike discharge characteristics.

Identification of four major cell classes in cat area 17

By examining a subset of easily quantified variables, we were able to propose relatively simple schemes that allow for the classification of cells in one of the four major classes. First, the neurons are segregated into bursting and nonbursting neurons based on the presence of two distinct bumps in the distribution of the logarithm of the ISIs (Fig. 2). The first represents ISIs that occur within the burst of spikes and the second is the interval between bursts (or between bursts and single spikes). This simple method, validated by discriminant analysis, reliably distinguishes RS and FS cells from IB and CH neurons. Preliminary analysis indicates that a similar classification can be achieved by analyzing the spike discharges obtained in response to sensory stimulation (Azouz et al. 1996).

Burst generation typically results from a fast ADP that is large enough to trigger an additional spike at short latency. Bursts are usually followed by a lengthy burst refractory period that is responsible for the gap between modes (Figs. 1, 2, and 9). Our definition of a burst is slightly different from those often used in *in vivo* studies, where a burst is referred to as the occurrence of a transitory high firing rate or a brief period of short interspike intervals (e.g., Bowman et al. 1995; DeBusk et al. 1997; Martinez-Conde et al. 2000). Our definition allowed us to exclude possible false positives, such as FS neurons with very high firing rates having ISI distributions that are confined to a narrow range of values. In such cases, the corresponding ISIH would not be bimodal (Fig. 2). Hence, by our definition, a cell that fires at a high rate is not necessarily a burst-generating neuron.

Following the segregation into bursting and nonbursting neurons, we found that multiple variables were required to reliably distinguish between cell classes; single variables, such as action potential width, were not sufficient as they exhibited considerable overlap between unique populations (e.g., Figs. 4 and 7–10). IB neurons could be distinguished from CH cells by either of the following two-variable criteria: CH cells are those bursting neurons that exhibit intraburst frequencies >350 Hz and spike widths of <0.5 ms (Fig. 9C). This criterion is useful, since it may be applied to extracellularly recorded bursting cells. Another two-variable criterion that reliably distinguishes between CH and IB neurons is that all CH cells have intraburst firing rates >350 Hz and burst inactivation indices of $<70\%$, while only two IB cells fell into this category (Fig. 10, B and C). This test for the identification of CH cells, however, requires the intracellular injection of constant current pulses, and therefore is less flexible.

Spike width and the degree of spike frequency adaptation were the two parameters that best distinguished RS and FS cells from one another: 92% of the cells that exhibit spike width of <0.5 ms at half-amplitude and an adaptation index of $<35\%$ can be reliably identified as FS cells (Fig. 8C). Again, this test for the identification of FS and RS cells requires the intracellular injection of constant current pulses. Although not examined here, the response to synaptic activation of FS neurons and RS cells that have thin spikes may be significantly different (Swadlow 1995) and therefore form a useful parameter for separation of these two cell types in extracellular recording studies despite overlapping action potential width.

Classical intrinsic bursting neurons

Numerous *in vivo* and *in vitro* studies performed in a wide variety of cortical areas and different species have examined the morphological and electrophysiological properties of neurons that are similar to our IB cells (Agmon and Connors 1989; Baranyi et al. 1993a; Chagnac-Amitai et al. 1990; Connors et al. 1982; Dégenétais et al. 2002; Franceschetti et al. 1995; Jones and Heinemann 1988; Mason and Larkman 1990; McCormick et al. 1985; Nuñez et al. 1993; Pockberger 1991; Silva et al. 1991; Steriade et al. 2001; Tseng and Prince 1993; Wang and McCormick 1993; traditional IB neurons have yet to be demonstrated in the human neocortex).

Morphologically, IB cells are typically pyramidal neurons whose cell bodies lie within layer 5 (Fig. 15A) with an apical dendrite extending up to layer 1 and horizontal axon collaterals

in the infragranular layers (Chagnac-Amitai et al. 1990; Franceschetti et al. 1995; Larkman and Mason 1990; McCormick et al. 1985; Wang and McCormick 1993). At least some layer 5 IB neurons project to the pontine nuclei and/or the superior colliculus and have the morphological features of corticopontine and corticotectal projecting neurons (Hübener et al. 1990; Kasper et al. 1994a; Wang and McCormick 1993). IB neurons have also been recorded in layers 2/3 and in layer 6, although their prevalence in these layers is lower than in layer 5 (see also Chen et al. 1996a; Dégenétais et al. 2002; Montoro et al. 1988; Nishimura et al. 2001; Pockberger 1991; van Brederode and Snyder 1992). Electrophysiologically, IB neurons generate bursts of spikes through the activation of an afterdepolarization following each action potential. In vitro studies have suggested that post spike ADP and burst generation by layer 3 and 5 pyramidal cells is likely to result from the activation of intrinsic depolarizing Na^+ currents by the action potentials within the burst (Franceschetti et al. 1995; Nishimura et al. 2001).

Our cluster analysis revealed the presence of three subclasses of IB neurons (Fig. 6). No single variable included in our analysis cleanly separated these three subclasses. Rather, a combination of at least two variables (spike width and intraburst frequency or spike width and burst inactivation index) was required. Our measure of burst-inactivation, although useful in separating these three clusters in combination with intraburst frequency and spike width, did not cleanly distinguish between these subgroups by itself, suggesting that the degree of burst inactivation varies along a continuum in IB cells. Nevertheless, IB1 and IB3 neurons display inactivating bursts, as is commonly observed in vitro, while IB2 neurons showed more of a repetitive burst discharge, a feature that is often observed in vivo (Baranyi et al. 1993a; Dégenétais et al. 2002; Nuñez et al. 1993; Steriade et al. 2001). The functional and anatomical correlates of these tentative subdivisions of IB neurons remains to be explored.

Chattering cells

Chattering cells generate repetitive bursts of thin (<0.55 ms) action potentials having intraburst firing rates in excess of 350 Hz. A similar pattern of action potential generation has been recorded intracellularly in the somatosensory cortex of the Raccoon in vivo (Istvan and Zarzecki 1994) and of cat in vitro (Kitagawa et al. 1999), in the visual cortex of the ferret in vitro (Brumberg et al. 2000), in cat association areas 5, 7, and 21 of the suprasylvian gyrus (Steriade et al. 1998), and in somatosensory and association cortical areas of unanesthetized cat (Steriade et al. 2001). In addition, the generation of high-frequency (>300 Hz) bursts of action potentials through intrinsic ionic mechanisms has been observed in cat pyramidal and nonpyramidal tract neurons of the motor cortex, in either anesthetized (Calvin and Sybert 1976; Steriade et al. 1998) or awake cats (Baranyi et al. 1993; Steriade et al. 2001), or in slices (Kitagawa et al. 1999). A pattern of action potential generation nearly identical to that reported here for CH cells can be observed in extracellular single unit studies in both awake and anesthetized primate and feline visual cortical areas in response to visual stimulation (Friedman-Hill et al. 2000; Gray and Viana Di Prisco 1997; Gray et al. 1990; Livingstone 1996). We are unaware of recordings demonstrating CH cells

in the rodent cerebral cortex, although this negative evidence does not exclude their existence in these animals.

The two subcategories of CH cells that we identified by cluster analysis could be distinguished from each other on the basis of intraburst firing rate and spike width. We have not found any physiological or functional correlates of these two subclasses of CH neurons.

The majority of CH neurons that we have morphologically identified were layer 2/3 pyramidal cells with simple receptive fields, suggesting that these cells may be monosynaptically innervated by thalamic Y-type afferents (Bullier and Henry 1979) and thus be involved in fast transfer of visual signals between different cortical areas. The number of projection sites targeted by lower layer 2/3 neurons is large, and includes ipsilateral cortical areas 18, 19, 21a, AMLS, PMLS, and PLLS (Bullier et al. 1984; Einstein and Fitzpatrick 1991; Symonds and Rosenquist 1984), as well as diverse cortical areas in the contralateral hemisphere (Innocenti 1980; Segraves and Rosenquist 1982; Voigt et al. 1988). It remains to be established whether CH cells target specifically some of these projection sites, or whether they project indiscriminately to all of these. In primate visual cortex, extracellular recording also revealed the presence of cells that fire high-frequency bursts of action potentials, often at frequencies within the gamma band (Friedman-Hill et al. 2000; Livingstone 1996). Similar to our observations in cat area 17, Livingstone (1996) found that one-half of the cells in layer 4B (which, in terms of connectivity, may be considered as part of the supragranular layers) and a majority of cells in the deep part of layer 2/3 display this discharge pattern.

It is not yet clear why CH cells are mostly observed in the supragranular layers in primary visual cortex, while in the suprasylvian gyrus, a CH-like behavior has been observed in pyramidal neurons of both supra- and infragranular layers, including corticothalamic neurons (and reportedly, in 1 "local circuit, sparsely spiny neuron") (Steriade et al. 1998). One key feature of CH cells is the generation of a fast spike ADP, which allows for the initiation of each additional action potential within the burst. In vitro, it has been found that pyramidal neurons that generate action potentials with prominent fast ADPs may be induced to "chatter" with repetitive or prolonged current injection, a process that is facilitated by some modulatory neurotransmitters (Brumberg et al. 2000; Kang and Kayano 1994; McCormick and Nowak 1996). This suggests that chattering, at least in some neurons, may represent more of a state of action potential generation than a cell type. However, in this study we did not observe any of the identified CH cells to spontaneously revert to non-CH neurons, even in the lack of visual stimulation or current injection. This finding suggests that a core group of neurons may generate action potentials largely or exclusively in the CH mode and therefore deserve the label "chattering cells," while other neurons may discharge in the CH mode during restricted periods of activation. Therefore it must be kept in mind that some neurons identified as CH may switch to a RS mode of action potential generation under certain circumstances (and vice versa).

In motor cortex, the generation of repetitive, high-frequency (>300 Hz) bursts has been observed in pyramidal tract neurons of the motor cortex in anesthetized (Calvin and Sybert 1976) and awake cat (Baranyi et al. 1993a), as well as in slices (Stafstrom et al. 1984). It is not clear whether these cells would

end up in a CH cell cluster, or whether some of their firing properties (for instance, their shallow f - I slope, Calvin and Sypert 1976) would attract them into a different cluster.

The presence of CH cells has rarely been reported in *in vitro* studies. Beside the possibility that CH cells may not exist in all animal species, it has been shown that the prevalence of CH cells *in vitro* is greatly increased by reducing the concentration of Ca^{2+} in the bathing medium to near that found *in vivo* (i.e., 1.2 mM), as well as by using adult animals (Brumberg et al. 2000). Because *in vitro* studies are typically conducted using Ca^{2+} concentrations at or near 2 mM, this may provide one explanation for the absence of CH cells from *in vitro* studies. By using cortical tissue from adult ferrets, the electrophysiological features of chattering cells have been examined. Chattering results from the generation of a postspike ADP, which is generated by the activation of a persistent sodium current by each action potential of the burst (Brumberg et al. 2000), possibly in a site remote from the site of spike generation (Wang 1999).

Extracellular recording studies in visual cortex have established a correlation between the presence of CH like discharge and the occurrence of gamma range oscillations (Friedman-Hill et al. 2000; Gray and Singer 1989; Gray et al. 1990; Livingstone 1996). Chattering cells are characterized by intrinsic generation of rhythmic bursting at 10–80 Hz, increasing with increasing current intensity (Fig. 11). This endogenous ability may play a key role in the generation of synchronized gamma frequency oscillations in networks of cortical neurons. Modeling studies have shown that cells with discharge properties similar to those of CH cells, when connected in a realistic fashion between each other and with FS cells, can generate synchronized oscillatory activity even if the “subcortical” synaptic input that drives the network is random (e.g., Bush and Sejnowski 1996). These findings suggest an important role of CH cells in the generation and communication of higher frequency oscillations in cortical networks.

Regular spiking cells

Regular spiking cells were characterized by the generation of tonic trains of action potentials (with fewer than 5% of their spikes in bursts) that showed spike frequency adaptation, and had spike widths that were broader on *average* than those of FS or CH neurons. Within the category of RS neurons, we also found two distinct subclasses that could be separated from one another according to spike width and their degree of spike-frequency adaptation. Thin spiking RS cells (RS_{TS}) are distinct from “classical” RS cells (RS_{C}) in that the former generated briefer action potentials and exhibited less spike frequency adaptation (see Fig. 8). Using criteria of more than 0.5 ms spike width at half height and an adaptation index larger than 60% allows a relatively good distinction between these two subclasses (Fig. 8C).

The intracellular injection of biocytin revealed RS cells to represent a wide variety of spiny neurons including pyramidal cells in layers 2–6, spiny stellate cells in layer 4, and polymorphic cells in layer 6. Other investigations *in vitro* have shown that some subtypes of inhibitory interneuron may discharge action potentials in a manner similar to the RS category defined here (see *Fast spiking cells*). Thus the “regular spiking” pattern of action potential generation appears to be widely

distributed among cells of different anatomical and functional properties, including pyramidal cells, spiny stellate neurons, and some subtypes of local inhibitory interneuron.

Fast spiking cells

Previously, McCormick et al. (1985) defined FS cells as those neurons that respond to depolarizing current pulses with a tonic train of relatively short-duration action potentials that exhibit little spike frequency adaptation and a relatively steep f - I relation. FS cells were shown to be local, presumed GABAergic, interneurons, and all morphological studies of FS neurons have since confirmed this finding. The morphological properties of FS neurons in this and a related study (Azouz et al. 1997) confirms them to be sparsely spiny or aspiny multipolar cells (basket and “clutch” cells), as observed in other studies (Chen et al. 1996a; Foering et al. 1991; Gupta et al. 2000; Hirsch 1995; Kawaguchi 1995; Neagele and Katz 1990; Thomson et al. 1996; Zhou and Hablitz 1996). FS cells have also been shown to correspond to parvalbumin containing cells (Cauli et al. 1997; Kawaguchi and Kubota 1997). Although McCormick et al. (1985) correctly predicted that FS cells are GABAergic, they did not state that the opposite was true. Indeed, they suggested that other types of GABAergic neurons may have their own electrophysiological properties, a prediction that subsequent studies have confirmed and expanded on (see below).

Our cluster analysis has confirmed the distinct nature of the FS classification of GABAergic interneurons and has shown that two distinct subcategories of FS cells can be discerned. Forty-five percent of the fast spiking cells (“classical” FS cells, FS_{C}) displayed f - I slopes larger than 320 Hz/nA, while the other class (FS_{LFI}) displayed f - I slopes lower than 320 Hz/nA. Unexpectedly, FS_{C} cells exhibited a very short membrane time constant.

Recent *in vitro* studies investigated the electrophysiological properties of diverse classes of GABAergic cells, which exhibit a wide variety of action potential discharge patterns. In addition to traditional FS neurons, nonpyramidal cells have also been categorized into other classes on the basis of their electrophysiological properties and in correlation with their pattern of axonal arbor, their synaptic properties, and their neurotransmitter and calcium binding proteins (Cauli et al. 1997, 2000; Foehring et al. 1991; Gibson et al. 1999; Gupta et al. 2000; Krimer and Goldman-Rakic 2001; Hestrin and Armstrong 1996; Hirsch 1995; Kawaguchi 1995; Kawaguchi and Kubota 1997; Llinas et al. 1991; Steriade et al. 1998; Thomson et al. 1996). None of the cells we recovered displayed morphological features of bipolar, bitufted, or double bouquet interneurons. Nor were they of the form of Martinotti or neurogliaform cells. The electrophysiological properties of these morphological subtypes of cells in adult cat area 17 *in vivo* remain to be examined. The high incidence of FS discharge pattern among our recordings of interneurons may result from the sampling bias of the intracellular recording technique. Parvalbumin containing interneurons (basket and chandelier cells) seem to be the dominant species of inhibitory cell in the cortex (37–74% of the GABAergic neurons, depending on the study and the species studied; Chow et al. 1999; Demeulemeester et al. 1991; Gonchar and Burkhalter 1997; Kawaguchi and Kubota 1997; Schwark and Li 2000; Van

Brederode et al. 1990). In addition, the cell bodies of parvalbumin containing interneurons are often larger than those of other types of interneurons (Schwark and Li 2000), which may allow these to be impaled more often. Finally, it is also possible that we recorded some non-FS interneurons but did not label them.

Recent studies (Chen et al. 1996b; Erisir et al. 1999) have shown that specific potassium channels, whose distribution seems to be restricted to the FS cell class (Chow et al. 1999), are responsible for both the narrow spikes and the ability of these cells to discharge at high sustained firing rate. It is tempting to propose that in other mammals, such as cats, RS_{TS} and CH cells, which generate short-duration action potentials, may have acquired a similar type and density of K⁺ channels as FS cells.

CONCLUSIONS

We have quantitatively justified the existence of four major electrophysiologically defined classes of neurons within the cat visual cortex and have presented simple methods to reliably classify neurons into these classes. Our classification scheme is based on intracellular recordings in area 17 of the cat *in vivo*, but is likely to hold generally throughout different mammalian species under a variety of conditions.

We thank F. Leniart and M. Sum for assistance in some of the histologies, J. Brumberg for assistance in some of the surgical preparations, and L. Rognlie-Howes for excellent care of the animals. We thank J. Bullier for helpful comments on the manuscript.

This work was supported by grants from the National Eye Institute to D. A. McCormick and C. M. Gray, the Fyssen Foundation, the Phillippe Foundation, Centre National de la Recherche Scientifique to L. G. Nowak, and the Human Frontiers Science Program Organization to R. Azouz.

Present address for R. Azouz: Dept. of Physiology, Zlotowski Center for Neuroscience, Ben-Gurion University, Beer-Sheva 84105, Israel.

REFERENCES

- Agmon A and Connors BW. Repetitive burst-firing neurons in the deep layers of mouse somatosensory cortex. *Neurosci Lett* 99: 137–141, 1989.
- Ahmed B, Anderson JC, Douglas RJ, Martin KAC, and Whitteridge D. Estimates of the net excitatory currents evoked by visual stimulation of identified neurons in cat visual cortex. *Cereb Cortex* 8: 462–476, 1998.
- Ahmed B, Anderson JC, Martin KAC, and Nelson JC. Map of the synapses onto layer 4 basket cells of the primary visual cortex of cat. *J Comp Neurol* 380: 230–242, 1997.
- Azouz R, Gray CM, Nowak LG, and McCormick DA. Physiological properties of inhibitory interneurons in cat striate cortex. *Cereb Cortex* 7: 534–545, 1997.
- Azouz R, Nowak LG, McCormick DA, and Gray CM. Multiparametric analysis of intracellular recordings in the cat striate cortex *in vivo* reveal four distinct cell classes. *Soc Neurosci Abst* 22: 633.14, 1996.
- Bair W, Koch C, Newsome W, and Britten K. Power spectrum analysis of bursting cells in area MT in the behaving monkey. *J Neurosci* 14: 2870–2892, 1994.
- Baranyi A, Szente MB, and Woody CD. Electrophysiological characterization of different types of neurons recorded *in vivo* in the motor cortex of the cat. I. Patterns of firing activity and synaptic responses. *J Neurophysiol* 69: 1850–1864, 1993a.
- Baranyi A, Szente MB, and Woody CD. Electrophysiological characterization of different types of neurons recorded *in vivo* in the motor cortex of the cat. II. Membrane parameters, action potentials, current-induced voltage responses and electrotonic structure. *J Neurophysiol* 69: 1865–1879, 1993b.
- Bernander Ö, Douglas RJ, Martin KAC, and Koch C. Synaptic background activity influences spatiotemporal integration in single pyramidal cells. *Proc Natl Acad Sci USA* 88: 11569–11573, 1991.
- Bowman DM, Eggermont JJ, and Smith GM. Effect of stimulation on burst firing in cat auditory cortex. *J Neurophysiol* 74: 1841–1855, 1995.
- Brumberg JC, Nowak LG and McCormick DA. Ionic mechanisms underlying repetitive high frequency burst firing in supragranular cortical neurons. *J Neurosci* 20: 4829–4843, 2000.
- Bullier J and Henry GH. Laminar distribution of first-order neurons and afferent terminals in cat striate cortex. *J Neurophysiol* 42: 1271–1281, 1979.
- Bullier J, Kennedy H, and Salinger W. Branching and laminar origin of projections between visual cortical areas in the cat. *J Comp Neurol* 228: 329–341, 1984.
- Bush P and Sejnowski T. Inhibition synchronizes sparsely connected cortical neurons within and between columns in realistic network model. *J Comput Neurosci* 3: 91–110, 1996.
- Calvin WH and Sypert GW. Fast and slow pyramidal tract neurons: an intracellular analysis of their contrasting repetitive firing properties in the cat. *J Neurophysiol* 39: 420–434, 1976.
- Cattaneo A, Maffei L, and Morrone C. Patterns in the discharge of simple and complex visual cortical cells. *Proc R Soc Lond B* 212: 279–297, 1981.
- Cauli B, Audinat E, Lambollez B, Angulo MC, Ropert N, Tsuzuki K, Hestrin S, and Rossier J. Molecular and physiological diversity of cortical nonpyramidal cells. *J Neurosci* 15: 3894–3906, 1997.
- Cauli B, Porter JT, Tsuzuki K, Lambollez B, Rossier J, Quenet B, and Audinat E. Classification of fusiform neocortical interneurons based on unsupervised clustering. *Proc Nat Acad Sci USA* 97: 6144–6149, 2000.
- Chagnac-Amitai Y, Luhmann HJ, and Prince DA. Burst generating and regular spiking layer 5 pyramidal neurons of rat neocortex have different morphological features. *J Comp Neurol* 296: 598–613, 1990.
- Chen W, Zhang J-J, Hu G-Y, and Wu C-P. Electrophysiological and morphological properties of pyramidal and nonpyramidal neurons in the cat motor cortex *in vitro*. *Neurosci* 73: 39–55, 1996a.
- Chen W, Zhang J-J, Hu G-Y, and Wu C-P. Different mechanisms underlying the repolarization of narrow and wide action potentials in pyramidal cells and interneurons of cat motor cortex. *Neurosci* 73: 57–68, 1996b.
- Chow A, Erisir A, Farb C, Nadal MS, Ozaita A, Lau D, Welker E, and Rudy B. K⁺ channel expression distinguishes subpopulations of parvalbumin- and somatostatin-containing neocortical interneurons. *J Neurosci* 19: 9332–9345, 1999.
- Connors BW, Gutnick MJ, and Prince DA. Electrophysiological properties of neocortical neurons *in vitro*. *J Neurophysiol* 48: 1302–1320, 1982.
- DeBusk BC, DeBruyn EJ, Snider RK, Kabara JF, and Bonds AB. Stimulus-dependent modulation of spike burst length in cat striate cortical cells. *J Neurophysiol* 78: 199–213, 1997.
- Dégenétais E, Thierry AM, Glowinski J, and Gioanni Y. Electrophysiological properties of pyramidal neurons in the rat prefrontal cortex: an *in vivo* intracellular recording study. *Cereb Cortex* 12: 1–16, 2002.
- Demeulemeester H, Arckens L, Vandesande F, Orban GA, Heizmann CW, and Pochet R. Calcium binding proteins and neuropeptides as molecular markers of GABAergic interneurons in the cat visual cortex. *Exp Brain Res* 84: 538–544, 1991.
- Deschênes M, Labelle A, and Landry P. Morphological characterization of slow and fast pyramidal tract cells in the cat. *Brain Res* 178: 251–274, 1979.
- Destexhe A and Pare D. Impact of network activity on the integrative properties of neocortical pyramidal neurons *in vivo*. *J Neurophysiol* 81: 1531–1547, 1999.
- Einstein G and Fitzpatrick D. Distribution and morphology of area 17 neurons that project to the cat's extrastriate cortex. *J Comp Neurol* 303: 132–149, 1991.
- Erisir A, Lau D, Rudy B, and Leonard CS. Function of specific K⁺ channels in sustained high-frequency firing of fast-spiking neocortical interneurons. *J Neurophysiol* 82: 2476–2489, 1999.
- Foehring RC, Lorenzon NM, Herron P, and Wilson CJ. Correlation of physiologically and morphologically identified neuronal types in human association cortex *in vitro*. *J Neurophysiol* 66: 1825–1837, 1991.
- Franceschetti S, Guatteo E, Panzica F, Sancini G, Wanke E, and Avanzini G. Ionic mechanisms underlying burst firing in pyramidal neurons: intracellular study in rat sensorimotor cortex. *Brain Res* 696: 127–139, 1995.
- Friedman-Hill S, Maldonado PE, and Gray CM. Dynamics of striate cortical activity in the alert monkey: I. Incidence and stimulus-dependence of gamma-band neuronal oscillations. *Cereb Cortex* 10: 1105–1116, 2000.
- Gibson JR, Beierlein M, and Connors BW. Two networks of electrically coupled inhibitory neurons in neocortex. *Nature* 402: 75–79, 1999.
- Gilbert CD. Laminar differences in receptive field properties of cells in cat primary visual cortex. *J Physiol* 268: 391–421, 1977.
- Gilbert CD and Wiesel TN. Morphology and intracortical projections of functionally characterised neurones in the cat visual cortex. *Nature* 280: 120–125, 1979.

- Gonchar Y and Burkhalter A.** Three distinct families of GABAergic neurons in rat visual cortex. *Cereb Cortex* 7: 347–358, 1997.
- Gray CM, Engel AK, König P, and Singer W.** Stimulus-dependent neuronal oscillations in cat visual cortex: receptive field properties and feature dependence. *Eur J Neurosci* 2: 607–619, 1990.
- Gray CM and McCormick DA.** Chattering cells: superficial pyramidal neurons contributing to the generation of synchronous oscillations in the visual cortex. *Science* 274: 109–113, 1996.
- Gray CM and Singer W.** Stimulus-specific neuronal oscillations in orientation columns of cat visual cortex. *Proc Natl Acad Sci USA* 86: 1698–1702, 1989.
- Gray CM and Viana Di Prisco G.** Stimulus dependent neuronal oscillations and local synchronization in striate cortex of the alert cat. *J Neurosci* 17: 3239–3253, 1997.
- Gupta A, Wang Y, and Markram H.** Organizing principles for a diversity of GABAergic interneurons and synapses in the neocortex. *Science* 287: 273–278, 2000.
- Hansen AK.** Effect of anoxia on ion distribution in the brain. *Physiol Rev* 65: 101–148, 1985.
- Hestrin A and Armstrong WE.** Morphology and physiology of cortical neurons in layer 1. *J Neurosci* 16: 5290–5300, 1996.
- Hirsch JA.** Synaptic integration in layer 4 of the ferret visual cortex. *J Physiol* 483: 183–199, 1995.
- Hirsch JA, Martinez LM, Alonso J-M, Pillai C, and Pierre C.** Simple and complex inhibitory cells in layer 4 of cat visual cortex. *Soc Neurosci Abstr* 26:1083, 2000.
- Horikawa K and Armstrong WE.** A versatile means of intracellular labeling: injection of biocytine and its detection with avidin conjugates. *J Neurosci Methods* 25: 1–11, 1988.
- Hubel DH and Wiesel TN.** Receptive fields, binocular interaction and functional architecture in the cat's visual cortex. *J Physiol* 160: 106–154, 1962.
- Hübener M, Schwarz C, and Bolz J.** Morphological types of projection neurons in layer 5 of cat visual cortex. *J Comp Neurol* 301: 655–674, 1990.
- Innocenti GM.** The primary visual pathway through the corpus callosum: morphological and functional aspects in the cat. *Arch Ital Biol* 118: 124–188, 1980.
- Istvan PJ and Zarzecki P.** Intrinsic discharge patterns and somatosensory inputs for neurons in raccoon primary somatosensory cortex. *J Neurophysiol* 72: 2827–2839, 1994.
- Jones RSG and Heinemann U.** Synaptic and intrinsic responses of medial entorhinal cortical cells in normal and magnesium-free medium in vitro. *J Neurophysiol* 59: 1476–1496, 1988.
- Kaneko T, Kang Y, and Mizuno N.** Glutaminase-positive and glutaminase-negative pyramidal cells in layer VI of the primary motor and somatosensory cortices: a combined analysis by intracellular staining and immunocytochemistry in the rat. *J Neurosci* 15: 8362–8377, 1995.
- Kang Y and Kayano F.** Electrophysiological and morphological characteristics of layer VI pyramidal cells in the cat motor cortex. *J Neurophysiol* 72: 578–591, 1994.
- Kasper EM, Larkman AU, Lubke J, and Blakemore C.** Pyramidal neurons in layer 5 of the rat visual cortex. I. Correlation among cell morphology, intrinsic electrophysiological properties, and axon target. *J Comp Neurol* 339: 459–474, 1994a.
- Kasper EM, Larkman AU, Lubke J, and Blakemore C.** Pyramidal neurons in layer 5 of the rat visual cortex. II. Development of electrophysiological properties. *J Comp Neurol* 339: 475–494, 1994b.
- Katz LC.** Local circuitry of identified projection neurons in cat visual cortex brain slices. *J Neurosci* 7: 1223–1249, 1987.
- Kawaguchi Y.** Physiological subgroups of nonpyramidal cells with specific morphological characteristics in layer II/III of rat frontal cortex. *J Neurosci* 15: 2638–2655, 1995.
- Kawaguchi Y and Kubota Y.** GABAergic cell subtypes and their synaptic connections in rat frontal cortex. *Cereb Cortex* 7: 476–486, 1997.
- Kisvárdy ZF, Martin KAC, Whitteridge D, and Somogyi P.** Synaptic connections of intracellularly filled clutch cells: a type of small basket cell in the visual cortex of the cat. *J Comp Neurol* 241: 111–137, 1985.
- Kitagawa H, Nishimura Y, and Yamamoto T.** Synaptic excitability of the burst firing neurons in cat sensorimotor cortex in vitro. *Brain Res* 842: 101–108, 1999.
- Krimer LS and Goldman-Rakic PS.** Prefrontal microcircuits: membrane properties and excitatory input to local, medium, and wide arbor interneurons. *J Neurosci* 21: 3788–3796, 2001.
- Larkman A and Mason A.** Correlations between morphology and electrophysiology of pyramidal neurons in slices of rat visual cortex. I. Establishment of cell classes. *J Neurosci* 10: 1407–1414, 1990.
- Leventhal AG and Hirsch HVB.** Receptive field properties of neurons in different laminae of visual cortex of the cat. *J Neurophysiol* 41: 948–962, 1978.
- Livingstone MS.** Oscillatory firing and interneuronal correlations in squirrel monkey striate cortex. *J Neurophysiol* 75: 2467–2485, 1996.
- Llinas RR, Grace AA, and Yarom Y.** In vitro neurons in mammalian cortical layer 4 exhibit intrinsic oscillatory activity in the 10- to 50-Hz frequency range. *Proc Natl Acad Sci USA* 88: 897–901, 1991.
- Mason A and Larkman A.** Correlations between morphology and electrophysiology of pyramidal neurons in slices of rat visual cortex. II. Electrophysiology. *J Neurosci* 10: 1415–1428, 1990.
- Martin KAC, Somogyi P, and Whitteridge D.** Physiological and morphological properties of identified basket cells in the cat's visual cortex. *Exp Brain Res* 50: 193–200, 1983.
- Martin KAC and Whitteridge D.** Form, function and intracortical projections of spiny neurones in the striate visual cortex of the cat. *J Physiol* 353: 463–504, 1984.
- Martinez-Conde S, Macknik SL, and Hubel DH.** Microsaccadic eye movements and firing of single cells in the striate cortex of macaque monkeys. *Nat Neurosci* 3: 251–258, 2000.
- Massimini M and Amzica F.** Extracellular calcium fluctuations and intracellular potentials in the cortex during the slow sleep oscillation. *J Neurophysiol* 85: 1346–1350, 2001.
- McCormick DA, Connors BW, Lighthall JW, and Prince DA.** Comparative electrophysiology of pyramidal and sparsely spiny neurons of the neocortex. *J Neurophysiol* 54: 782–806, 1985.
- McCormick DA and Nowak LG.** Possible cellular mechanisms for arousal-induced higher frequency oscillations: acetylcholine and ACPD induce repetitive burst firing in visual cortical neurons. *Soc Neurosci Abstr* 22:644, 1996.
- McCormick DA and Prince DA.** Post-natal development of electrophysiological properties of rat cerebral cortical pyramidal neurones. *J Physiol* 393: 743–762, 1987.
- McCormick DA, Wang Z, and Huguenard J.** Neurotransmitter control of neocortical neuronal activity and excitability. *Cereb Cortex* 3: 387–393, 1993.
- Montoro RJ, Lopez-Barneo J, and Jassik-Gerschenfeld D.** Differential burst firing mode in neurons of mammalian visual cortex in vitro. *Brain Res* 460: 168–172, 1988.
- Mountcastle VB, Talbot WH, Sakata H, and Hyvärinen J.** Cortical neuronal mechanisms in flutter-vibration studied in unanesthetized monkeys. Neuronal periodicity and frequency discrimination. *J Neurophysiol* 32: 452–484, 1969.
- Neagele JR and Katz LC.** Cell surface molecules containing N-acetylgalactosamine are associated with basket cells and neurogliaform cells in cat visual cortex. *J Neurosci* 10: 540–557, 1990.
- Nishimura Y, Asahi M, Saitoh K, Kitagawa H, Kumazawa Y, Itoh K, Lin M, Akamine T, Shibuya H, Asahara T, and Yamamoto T.** Ionic mechanisms underlying burst firing of layer III sensorimotor cortical neurons of the cat: an in vitro slice study. *J Neurophysiol* 86: 771–781, 2001.
- Núñez A, Amzica F, and Steriade M.** Electrophysiology of cat association cortical cells in vivo: intrinsic properties and synaptic responses. *J Neurophysiol* 70: 418–435, 1993.
- Pockberger H.** Electrophysiological and morphological properties of rat motor cortex neurons in vivo. *Brain Res* 539: 181–190, 1991.
- Sanchez-Vives MV and McCormick DA.** Cellular and network mechanisms of rhythmic recurrent activity in neocortex. *Nature Neurosci* 3: 1027–1034, 2000.
- Sanchez-Vives MV, Nowak LG, and McCormick DA.** Membrane mechanisms underlying contrast adaptation in cat area 17 in vivo. *J Neurosci* 20: 4267–4285, 2000.
- Schiller PH, Finlay BL, and Volman SF.** Quantitative studies of single-cell properties in monkey striate cortex. I. Spatiotemporal organization of receptive fields. *J Neurophysiol* 39: 1288–1319, 1976.
- Schwark HD and Li J.** Distribution of neurons immunoreactive for calcium-binding proteins varies across areas of cat primary somatosensory cortex. *Brain Res Bull* 51: 379–385, 2000.
- Segraves MA and Rosenquist AC.** The afferent and efferent callosal con-

- nections of retinotopically defined areas in cat cortex. *J Neurosci* 2: 1090–1107, 1982.
- Silva LR, Amitai Y, and Connors BW.** Intrinsic oscillations of neocortex generated by layer 5 pyramidal neurons. *Science* 251: 432–435, 1991.
- Simons DJ.** Response properties of vibrissa units in rat S1 somatosensory neocortex. *J Neurophysiol* 41: 798–820, 1978.
- Skottun BC, De Valois RL, Grosf DH, Movshon JA, Albrecht DG, and Bonds AB.** Classifying simple and complex cells on the basis of response modulation. *Vision Res* 31: 1079–1086, 1991.
- Somogyi P.** A specific “axo-axonal” interneuron in the visual cortex of the rat. *Brain Res* 136: 345–350, 1977.
- Somogyi P, Kisvarday ZF, Martin KAC, and Whitteridge D.** Synaptic connections of morphologically identified and physiologically characterized large basket cells in the striate cortex of cat. *Neuroscience* 10: 261–294, 1983.
- Stafstrom CE, Schwindt PC, and Crill WE.** Repetitive firing in layer V neurons from cat neocortex in vitro. *J Neurophysiol* 52: 264–277, 1984.
- Steriade M, Timofeev I, Dürmüller N, and Grenier F.** Dynamic properties of corticothalamic neurons and local cortical interneurons generating fast rhythmic (30–40 Hz) spike bursts. *J Neurophysiol* 79: 483–490, 1998.
- Steriade M, Timofeev I, and Grenier F.** Natural waking and sleep states: a view from inside neocortical neurons. *J Neurophysiol* 85: 1969–1985, 2001.
- Swadlow HA.** Influence of VPM afferents on putative interneurons in S1 of the awake rabbit: evidence from cross-correlation, microstimulation, and latencies to peripheral sensory stimulation. *J Neurophysiol* 73: 1584–1599, 1995.
- Symonds LL and Rosenquist AC.** Laminar origins of visual corticocortical connections in the cat. *J Comp Neurol* 229: 39–47, 1984.
- Takahashi K.** Slow and fast groups of pyramidal tract cells and their respective membrane properties. *J Neurophysiol* 28: 908–924, 1965.
- Thomson AM, West DC, Hahn J, and Deuchars J.** Single axon IPSPs elicited in pyramidal cells by three classes of interneurons in slices of rat neocortex. *J Physiol* 496: 81–102, 1996.
- Tseng G-F and Prince DA.** Heterogeneity of rat corticospinal neurons. *J Comp Neurol* 335: 92–108, 1993.
- Van Brederode JFM, Mulligan KA, and Hendrickson AE.** Calcium-binding proteins as markers for subpopulations of GABAergic neurons in monkey striate cortex. *J Comp Neurol* 298: 1–22, 1990.
- Van Brederode JFM and Snyder GL.** A comparison of the electrophysiological properties of morphologically identified cells in layers 5B and 6 of the rat neocortex. *Neuroscience* 50: 315–337, 1992.
- Voigt T, LeVay S, and Stammes MA.** Morphological and immunocytochemical observations on the visual callosal projections in the cat. *J Comp Neurol* 272: 450–460, 1988.
- Wang XJ.** Fast burst firing and short-term synaptic plasticity: a model of neocortical chattering neurons. *Neuroscience* 89: 347–362, 1999.
- Wang Z and McCormick DA.** Control of firing mode of corticotectal and corticopontine layer V burst-generating neurons by norepinephrine, acetylcholine and 1S, 3R-ACPD. *J Neurosci* 13: 2199–2216, 1993.
- Zhou F-M and Hablitz JJ.** Layer I neurons of rat neocortex. I. Action potential and repetitive firing properties. *J Neurophysiol* 76: 651–667, 1996.